Nuclear Engineering Division
Nuclear Engineering Division
Nuclear Engineering Division
Nuclear Engineering Division
Nuclear Engineering Division
Nuclear Engineering Division
Nuclear Engineering Division
Nuclear Engineering Division
Nuclear Engineering Division
Nuclear Engineering Division
Nuclear Engineering Division
Nuclear Engineering Division
Nuclear Engineering Division
Nuclear Engineering Division
Nuclear Engineering Division
Nuclear Engineering Division
Nuclear Engineering Division
Nuclear Engineering Division
Nuclear Engineering Division
Nuclear Engineering Division
Nuclear Engineering Division
Nuclear Engineering Division
Nuclear Engineering Division

ANL-04-27

High Strength and Heat Resistant Chromium Steels for Sodium-Cooled Fast-Reactors

by S.A. Kamal, C.W. Grandy, M.T. Farmer, and A.R. Brunsvold

Argonne National Laboratory, Argonne, Illinois 60439
Operated by The University of Chicago
for the United States Department of Energy under Contract W-31-109-Eng-38

Nuclear Engineering Division
Nuclear Engineering Division
Nuclear Engineering Division
Nuclear Engineering Division
Nuclear Engineering Division
Nuclear Engineering Division
Nuclear Engineering Division
Nuclear Engineering Division
Nuclear Engineering Division
Nuclear Engineering Division
Nuclear Engineering Division
Nuclear Engineering Division
Nuclear Engineering Division
Nuclear Engineering Division
Nuclear Engineering Division
Nuclear Engineering Division
Nuclear Engineering Division

Argonne National Laboratory, a U.S. Department of Energy Office of Science laboratory, is operated by The University of Chicago under contract W-31-109-Eng-38.

DISCLAIMER

This report was prepared as an account of work sponsored by an agency of the United States Government. Neither the United States Government nor any agency thereof, nor The University of Chicago, nor any of their employees or officers, makes any warranty, express or implied, or assumes any legal liability or responsibility for the accuracy, completeness, or usefulness of any information, apparatus, product, or process disclosed, or represents that its use would not infringe privately owned rights. Reference herein to any specific commercial product, process, or service by trade name, trademark, manufacturer, or otherwise, does not necessarily constitute or imply its endorsement, recommendation, or favoring by the United States Government or any agency thereof. The views and opinions of document authors expressed herein do not necessarily state or reflect those of the United States Government or any agency thereof, Argonne National Laboratory, or The University of Chicago.

Available electronically at http://www.osti.gov/bridge/

Available for a processing fee to U.S. Department of Energy and its contractors, in paper, from:

U.S. Department of Energy
Office of Scientific and Technical Information
P.O. Box 62
Oak Ridge, TN 37831-0062
phone: (865) 576-8401
fax: (865) 576-5728
email: reports@adonis.osti.gov

ANL-04-27

HIGH STRENGTH AND HEAT RESISTANT CHROMIUM STEELS FOR SODIUM-COOLED FAST-REACTORS

S.A. Kamal, C.W. Grandy, M.T. Farmer, and A.R. Brunsvold

Nuclear Engineering Division
Argonne National Laboratory
9700 South Cass Avenue
Argonne, IL 60439

October 2004

TABLE OF CONTENTS

ABSTRACT 1

1.0 INTRODUCTION 2

2.0 SIMPLIFIED STEAM GENERATOR THERMAL AND STRESS COMPUTER PROGRAM 2
- 2.1 Thermal Model Development 3
- 2.2 Validation of Thermal Calculation Results 4
- 2.3 Stress, Strain, Deformation, and Weight Calculations 5
- 2.4 Calculation Results for Steam Generator Tubes Made of 2¼Cr-1Mo, 9Cr-1MoVNb, and 12Cr-2W Steels 6

3.0 DATABASE FOR ADVANCED FERRITIC STEELS 7
- 3.1 12Cr-2W Steel 10
- 3.2 9Cr-1MoVNb Steel 11

4.0 RECOMMENDED FOLLOW UP STEPS 11
- 4.1 Extending Material Database 12
- 4.2 Extending Computer Program Capability 12
- 4.3 Calculations with Advanced Ferritic Steels 13

REFERENCES 13

APPENDIX A: THERMAL-HYDRAULIC MODEL FOR SHELL-AND-TUBE SUPERHEATED STEAM GENERATOR 30

APPENDIX B: EVALUATION OF SIMPLIFIED THERMAL-HYDRAULIC MODEL FOR SHELL-AND-TUBE STEAM GENERATOR 48

LIST OF FIGURES

1. Modeling of Water/Steam Flow through Tube in Superheater Steam Generator 16

2. Temperature Distributions along a Steam Generator Tube Made of 2.25Cr-1Mo Steel 17

3. Allowable Stresses of 2.25Cr-1Mo, 9Cr-1MoVNb, and 12Cr-2W Steels 18

4. Coefficient of Thermal Expansion of 2.25Cr-1Mo, 9Cr-1MoVNb, and 12Cr-2W Steels 19

5. Modulus of Elasticity of 2.25Cr-1Mo, 9Cr-1MoVNb, and 12Cr-2W Steels 20

6. Thermal Conductivity of 2.25Cr-1Mo, 9Cr-1MoVNb, and 12Cr-2W Steels 21

7. Temperature Distributions along a Steam Generator Tube Made of 9Cr-1MoVNb Steel 22

8. Temperature Distributions along a Steam Generator Tube Made of 12Cr-2W Steel 23

9. Ratio of Tube Stress due to Internal Pressure to Material Allowable Stress 24

10. Ratio of Temperature Difference through Tube Wall to Material Fatigue Allowable Limit 25

LIST OF TABLES

1. Input Data Description of Computer Code HeatXchngr1 26

2. Comparison of Bench Mark Parameters and HX Model Results 28

3. Comparison of Input Parameters and Calculation Results for Steam Generator Tubes Made of 2.25Cr-1Mo, 9Cr-1MoVNb, and 12Cr-2W Steels 29

ACRONYMS

AFR	Advanced Fast Reactor
AI	Atomics International
ANL	Argonne National Laboratory
ASME	American Society of Mechanical Engineers
B&PV	Boiler and Pressure Vessel
ID	Inside Diameter
IHX	Intermediate Heat Exchanger
HX	Heat Exchanger
LDRD	Laboratory Directed Research and Development Program
OD	Outside Diameter
ORNL	Oak Ridge National Laboratory
OT	Once-Through (Steam Generator)
SCWR	Super-Critical Water Reactor
SG	Steam Generator
TS	Tube Side
VHTR	Very High Temperature Reactor
4S	Super Safe, Small, and Simple Liquid Metal Reactor

HIGH STRENGTH AND HEAT RESISTANT CHROMIUM STEELS FOR SODIUM-COOLED FAST-REACTORS

S.A. Kamal, C.W. Grandy, M.T. Farmer, and A.R. Brunsvold

ABSTRACT

This report provides the results of a preliminary phase of a project supporting the Advanced Nuclear Fuel Cycle Technology Initiative at ANL. The project targets the Generation IV nuclear energy systems, particularly the area of reducing the cost of sodium-cooled fast-reactors by utilizing innovative materials. The main goal of the project is to provide the nuclear heat exchanger designers a simplified means to quantify the cost advantages of the recently developed high strength and heat resistant ferritic steels with 9 to 13% chromium content. The emphasis in the preliminary phase is on two steels that show distinctive advantages and have been proposed as candidate materials for heat exchangers and also for reactor vessels and near-core components of Gen IV reactors. These steels are the 12Cr-2W (HCM12A) and 9Cr-1MoVNb (modified 9Cr-1Mo). When these steels are in tube form, they are referred to in ASTM Standards as T122 and T91, respectively.

A simple thermal-hydraulics analytical model of a counter-flow, shell-and-tube, once-through type superheated steam generator is developed to determine the required tube length and tube wall temperature profile. The single-tube model calculations are then extended to cover the following design criteria: (i) ratio of the tube stress due to water/steam pressure to the ASME B&PV Code allowable stress, (ii) ratio of the strain due to through-tube-wall temperature differences to the material fatigue limit, (iii) overall differential thermal expansion between the tube and shell, and (iv) total amount of tube material required for the specified heat exchanger thermal power. Calculations were done for a 292 MW steam generator design with 2200 tubes and a steam exit condition of 457°C and 16 MPa. The calculations were performed with the tubes made of the two advanced ferritic steels, 12Cr-2W and 9Cr-1MoVNb, and of the most commonly used steel, 2¼Cr-1Mo. Compared to the 2¼Cr-1Mo results, the 12Cr-2W tubes required 29% less material and the 9Cr-1MoVNb tubes required 25% less material. Also, with the advanced steels, the thermal strains in the tubes and differential thermal expansion between tubes and shell were significantly better. For steam generators with higher steam exit temperatures, the benefits of the advanced steels become much larger.

A thorough search for the thermal and mechanical properties of the two advanced steels was conducted. A summary of the search results is provided. It shows what is presently known about these two advanced steels and what still needs to be determined so that they can be used in nuclear heat exchanger designs. Possible follow up steps are outlined.

1. 0 INTRODUCTION

Over the last twenty five years, there has been an interest (in the United States and other countries) in the special properties of the 9 to13Cr steels which made them appropriate structural materials for power generation components built per ASME B&PV Code Section I (power boilers) and VIII, Division 1 (pressure vessels) for service temperatures up to 649°C. In addition, their high resistance to neutron-induced swelling made them appropriate materials for reactor core subassemblies and fuel pin cladding in sodium-cooled fast reactors. More recently, the potential nuclear applications of these materials has expanded as they become candidate materials for the reactor pressure vessel of the Gen IV VHTR, steam lines of SCWR, and core barrel and reflector of the 4S Japanese reactor. The use of the 12Cr-2W steel in the cooling system of a 1500 MWe commercial sodium-cooled Japanese reactor (Reference 1) was reportedly an important factor in demonstrating that the overall cost of this advanced nuclear power plant could be reduced to 2/3 the cost of a conventional light water reactor. This advantage of sodium-cooled reactors is extremely important in making these advanced reactors more favorable on an economical basis in addition to their recognized advantage of higher safety.

In order to utilize these steels in nuclear applications (pressure retaining boundaries or core support structures) at temperatures above 371°C, the component design has to meet the stringent requirements of the ASME Code Section III, Subsection NH (Reference 2). The 9Cr-1MoVNb steel, which was originally developed and tested at ORNL in the early 1980s, is expected to be approved this year for usage per this subsection of the ASME Code, Reference 3. However, the constitutive equations that would enable the performance of inelastic structural analysis and design evaluation are still being developed. The 12Cr-2W steel which appears to have superior properties was developed by Sumitomo Metal Industries, Ltd. of Japan. Although some data about this steel is available, an extensive testing program will be required in order to qualify this steel for nuclear service per ASME Code Subsection NH.

2.0 SIMPLIFIED STEAM GENERATOR THERMAL AND STRESS COMPUTER PROGRAM

A simple thermal-hydraulics analytical model of a classic counter-flow, shell-and-tube, once-through type superheated steam generator was developed to support the effort of assessing different types of steels for use in advanced reactor heat exchanger (HX) design applications. For a given HX thermal power level, HX inlet and exit conditions, and mechanical design characteristics (i.e., the number of tubes, tube thermal conductivity, pitch, diameter, and wall thickness), the model calculates the required HX tube length to achieve a specified superheated steam. The model also provides the bulk liquid metal (shell-side) temperature, bulk steam/water (tube-side) temperature, and the tube inner and outer surface temperatures as functions of distance along the HX tube length. The tube

length and tube wall temperature profile are key information needed to assess materials issues related to the HX design.

The single-tube model calculations were extended to cover tube stresses due to water/steam pressure (basis for tube wall thickness), thermal strains due to through- tube-wall temperature differences and overall differential thermal expansion between the tube and shell. Material corrosion, which is an important factor in steam generator design, was indirectly considered in the stress calculations by extracting an estimated corrosion allowance from the wall thickness. The model provides, along the tube length, the ratio of the tube stress to the material allowable limit and ratio of thermal strain to the material fatigue limit. The calculations also include the total amount of tube material required for the specified HX thermal power. Presently, the model material library covers the mechanical and thermal properties of the 12Cr-2W, 9Cr-1MoVNb, and 2¼Cr-1Mo steels. A FORTRAN computer program (HeatXchngr1) is written to perform the HX Model calculations. A brief description of the computer program input data is shown in Table 1.

The thermal, stress, strain, deformation, and weight simplified calculations of the program HeatXchngr1 provide the heat exchanger designers a useful tool to evaluate the advantages of advanced materials based on the entire properties of the material instead of just the allowable stress at the maximum operating temperature. Further development of the program to include, for instance, a corrosion model that takes cognizance of material test data and heat exchanger operating conditions would certainly enhance the program capability and value.

2.1 Thermal Model Development

The analytical modeling, described in detail in Appendix A, considers a single hydraulic sub-channel for a counter-flow, shell-and-tube type, superheated steam generator that is vertically oriented. The water flow is through the tube side of the HX while the liquid sodium flows through the shell side. The model assumes that the tube side is maintained at a uniform pressure which fixes the boiling point at the corresponding saturation temperature for the HX pressure. As shown in Figure 1, for each sub-channel of the HX, the feedwater is assumed to enter the single-wall tube from below at a specified subcooling relative to the saturation temperature. As the water flows through the channel, it is first heated by forced convection single-phase heat transfer to near the saturation temperature. Once the boiling point is reached, a two-phase boiling heat transfer region occurs in which the liquid-component of the steam/water mixture is steadily vaporized and the steam quality eventually reaches unity. Finally, another single phase flow region is encountered where the steam undergoes additional heating to a specified superheat relative to the saturation point at the HX exit. Individual models for each of these three flow regions are developed. In addition, simple expressions are developed to relate the sub-channel liquid metal and feedwater flow rates to the specified HX power level, as well as the specific enthalpy change of the water coolant as it flows through the HX.

2.2 Validation of Thermal Calculation Results

The calculation procedure and results of the HX thermal model were thoroughly and independently checked (see Appendix B). This effort was based on two considerations: (1) a comparison of the HX Model predicted general results to the results reported for a steam generator (SG) design with extensive development and testing program, bench mark results; and (2) evaluating the predicted behavior of the fluid and tube wall temperature distributions along the length of the steam generator for correct trends. The bench mark results were for a sodium-heated, once-through, counter-flow, hockey-stick, and single-wall tube steam generator configuration with water on the tube side (Reference 4). The unit which was designed specifically for once-through operating conditions was completed by Atomics International (AI) using the same tube size as that in the Clinch River Breeder Reactor steam generator modules. The active heat transfer region of the hockey-stick tube bundle is confined to the long leg of the steam generator. Thus, for heat transfer purposes, the hockey-stick can be correctly modeled as a straight tube unit.

A comparison of the results using the HX Model with those of AI-SG design is given in Table 2. The table is organized with parameters used as input to the HX Model given in the upper rows followed by those calculated by the HX Model. It is worth noting that the tube material in both cases was the 2¼Cr-1Mo ferritic steel (referred to in ASTM Standards as T22). A comparison of the Table 2 flow rates and the active heat transfer length shows the following:

<u>Sodium Flow Rate</u>

The sodium flows are very close with the HX Model predicting a flow that is larger than the AI-SG value by less than 1%.

<u>Water/Steam Flow Rate</u>

The HX Model predicts the water/steam flow rate to be about 8% larger than the AI-SG water/steam flow rate. This difference is attributed primarily to the differences in the water/steam properties used in the two studies which result from the simplifications made in the HX Model. The major simplifications in the HX Model are the assumption of constant water/steam side pressure and the use of constant specific heats at representative temperatures in the subcooled and superheated regions.

<u>Active Heat Transfer Length</u>

The HX Model predicts an active heat transfer length that is about 27% less than the length in the AI-SG design. This under-prediction by the HX Model is expected primarily because the HX Model does not include any allowances for uncertainties that were included in the AI-SG design. For instance the HX Model does not include allowances for tube plugging, ineffective heat transfer region where the tubes pass through support plates, or uncertainty about heat transfer coefficients.

Figure 2 shows the tube and both fluids temperature profiles along the active heat transfer length for the AI-SG calculated by the HX Model for the input given in Table 2. The main conclusion of the program validation effort is that the HX Model predicts reasonable results and the model can be used in trade-off and material comparison studies on this type of steam generators.

2.3 Stress, Strain, Deformation, and Weight Calculations

The two most important criteria in determining the suitability of a structural material for heat exchanger applications at elevated temperatures are the tube allowable stress and corrosion resistance. The use of a material with a higher allowable stress leads to a heat exchanger design with thinner tube wall and more efficient heat transfer across the tube wall and this in turn leads to a smaller tube bundle weight for the specified thermal power. Another two important criteria are the maximum thermal strain induced by through-the-wall temperature difference and its relation to the material fatigue limit at very high number of cycles and the overall differential thermal expansion between the tube bundle and the shell which the design has to accommodate.

In addition to the thermal calculations of the HX Model described in the previous subsections, the following calculations were added:

1. The tube circumferential stress (due to internal pressure) and its value relative to the material allowable stress as specified in the ASME B&PV Code;

2. The temperature difference through the tube wall and its value relative to the material allowable limit based on the fatigue strain at 10^8 cycles;

3. The differential thermal expansion between the tubes and the shell based on the difference between the average tube wall temperature and sodium temperature integrated along the entire length of the tube; and

4. The weight of the tube bundle.

Presently, the computer program (HeatXchngr1) provides as functions of tube temperature the allowable stress, coefficient of thermal expansion, modulus of elasticity, and thermal conductivity for 12Cr-2W, 9Cr-1MoVNb, and 2¼Cr-1Mo steels (see Figures 3 through 6). The program also provides a temperature independent fatigue limit and density for each of the three steels. The fatigue strain limits at 10^8 cycles for the three steels are as follows:

<u>2¼Cr-1Mo steel</u> 0.74×10^{-3} for temperatures ≤ 593°C
Extrapolated value based on design fatigue data given in Reference 2.

<u>9Cr-1MoVNb steel</u> 1.20×10^{-3}
Design fatigue data (at temperatures ≤ 538°C) given in References 3 and 5.

12Cr-2W steel 1.00×10^{-3}

Since there was no fatigue data available, an estimated value was used, approximately the average of the 2¼Cr-1Mo and 9Cr-1MoVNb values.

As mentioned earlier, the tube corrosion (on the water/steam side) is simply considered by subtracting a corrosion allowance (input data) from the tube wall thickness before determining the tube circumferential stress.

2.4 Calculation Results for Steam Generator Tubes Made of 2¼Cr-1Mo, 9Cr-1MoVNb, and 12Cr-2W Steels

As an example on how the HeatXchngr1 program can be used to assess the advantages of utilizing advanced ferritic steels in a steam generator design, the calculations that were done earlier to validate the program (see Subsection 2.2) are repeated with the tubes made of 9Cr-1MoVNb and 12Cr-2W steels instead of 2¼Cr-1Mo steel. As shown in Table 3, the following input parameters for the calculations with the advanced steels are maintained the same as in the reference case of 2¼Cr-1Mo steel:

1. Steam generator thermal power,
2. Inlet and outlet conditions of sodium and water/steam,
3. Number of tubes,
4. Tube inside diameter,
5. Ratio of tube pitch to tube outside diameter,
6. Corrosion allowance, and
7. Ratio of circumferential stress to allowable stress.

Figures 7 and 8 show the temperature profiles for steam generator tubes made of 9Cr-1MoVNb and 12Cr-2W, respectively. With the exception of slightly shorter tubes when the advanced steels are used, only small differences can be noticed between these profiles and those of the 2¼Cr-1Mo steel shown in Figure 2. Figure 9 compares the Stress Ratio (circumferential stress / the corresponding allowable stress) along the tube length for the two advanced steels and the reference steel. Similarly, Figure 10 compares the ΔT Ratio (temperature difference between OD and ID of the tube / allowable fatigue limit) along the tube length. The smaller ΔT Ratio of the advanced steels relative to that of the reference steel reflects the effect of smaller coefficients of expansion and larger fatigue limits for the advanced steels.

Focusing on the calculation results that directly relate to the design evaluation criteria (summarized in Table 3), one can easily see the following advantages of the advanced steel relative to the reference case of the 2¼Cr-1Mo steel:

1. The total weight of the 9Cr-1MoVNb tubes is 75% of the reference case and 71% of the reference case with 12Cr-2W tubes.

2. The ratio of the maximum ΔT through the wall to the fatigue allowable limit with the 9Cr-1MoVNb tubes is 54% of the reference case and 56% of the reference case with 12Cr-2W tubes.

3. The differential thermal expansion between the tube bundle and shell with the 9Cr-1MoVNb tubes is 82% of the reference case and 71% of the reference case with 12Cr-2W tubes.

The first advantage shows the obvious economical benefit of less material usage with the advanced steels. The second and third advantages lead to a longer service life for the component and consequently additional economical benefits are realized. It is worth mentioning that the above example does not show the full advantages of the two advanced steels for two reasons:

1. The level of the tube temperature was not high enough (about 475°C). At higher temperatures the use of the 2¼Cr-1Mo steel would have required a very large tube thickness because of the severe drop in the allowable stress (see the relation between the allowable stresses shown in Figure 3 at 475°C and 550°C).

2. The corrosion resistance of the advanced steels is conservatively assumed to be the same as that of the 2¼Cr-1Mo steel. Test data has shown (Reference 7) that the corrosion of these two steels is significantly less than that of the reference steel.

3.0 DATABASE FOR ADVANCED FERRITIC STEELS

According to a study of evolution of ferritic steels for boilers presented in Reference 6, the 12Cr-2W and 9Cr-1MoVNb are categorized as third and second generation ferritic steels, respectively. The third generation steels are defined as those steels that have 10^5 hour creep rupture strength at 600°C of 140 MPa and the second generation steels have creep rupture strength of 100 MPa. Whereas, the 2¼Cr-1Mo steel, the most commonly used steel for nuclear steam generators in the past, is in a category that has a creep strength of only 35 MPa. The 12Cr-2W and 9Cr-1MoVNb are to be used in normalized and tempered conditions and their welding, as with most ferritic steels, requires pre- and post-weld heat treatments. The results, thus far, of searching for the properties of the two steels are summarized in Subsection 3.1 and 3.2. Some data about the 12Cr-2W steel was obtained directly from the steel manufacturer, Reference 7. An advanced copy of the

2004 Subsection NH of the ASME B&PV Code, Reference 3, revealed that the new code revision would include a substantial amount of data about the 9Cr-1MoVNb steel.

Inelastic stress analyses are usually necessary in order to demonstrate that a steam generator design for a nuclear power plant meets the strain and deformation limits specified in Appendix T of ASME Subsection NH (Reference 2). There are two essential material behavior characteristics that are not addressed by the procedures of Subsection NH but they are required in performing such inelastic analyses. These two characteristics are: (i) effect of cyclic loading beyond yield stress on subsequent material behavior, and (ii) constitutive equations that describe how the creep and plastic strain increments are calculated in terms of the current stress state, stress increments, time increment, and temperature. For austenitic stainless steel Types 304 and 316 and ferritic steel 2¼Cr-1Mo, these characteristics have been fully addressed in numerous publications and there are structural analysis computer programs that incorporate such material behavior characteristics.

Insights into the unique and complex behavior of 9Cr-1MoVNb steel under cyclic loadings are given in Reference 8. The steel in the tests described in this reference was normalized at 1020°C, air cooled, tempered at 760°C for 2 h, and given a simulated post-weld heat treatment at 730°C for 20 h. Figure 2 in Reference 8 shows typical stress versus strain hysteresis loops (uniaxial cyclic loadings) for several temperatures and depicts the effect of strain rate on the first cycle loop at 550°C. Also, Figure 3 in the same reference shows how, in these cyclic loadings, the stress amplitude varies with strain amplitude and number of cycles at 500°C and 600°C. The two figures reveal the clear cyclic softening and additional softening that takes place as a result of increase in strain rate and amount of strain amplitude at higher temperatures. Figure 6, in the same reference, illustrates another aspect of material softening during creep tests at 500°C as a result of periodic fast stress reversal. Under a steady stress of 276 MPa (initial minimum yield stress at 500°C is 306 MPa), the estimated rupture time was 10^5 h. But when the stress was reversed to -276 MPa at a frequency of 12 cycles/h and a ramp time of 10 s, the creep rate accelerated and a creep failure occurred in 600 h. And when the frequency of load cycling increased to 100 cycles/h , the specimen showed much larger creep strain rate and failed in only 145 h.

As for the constitutive equations of 9Cr-1MoVNb steel, results of radial and non-radial loading tests performed at ORNL in the mid 1980s indicated (Reference 9) that (i) the von Mises yield criterion can be used as a basis for modeling initial yield behavior, (ii) subsequent yield behavior is more kinematic than isotropic, and (iii) non-uniform softening takes place leading to elliptically shaped yield locus that becomes smaller in the direction of loading. The ORNL researchers, however, concluded that the current creep-plasticity interaction rules were inadequate for modeling 9Cr-1MoVNb steel and recommended a nonlinear viscoplastic model which does not distinguish between creep and plastic strains. More recently, abstracts of articles published in Japanese by Yaguchi and Takahashi (References 10 and 11) indicate that progress has been made in developing constitutive equations based on a viscoplastic model that was capable of simulating strain-rate dependency at high temperatures (500°C and above) only; and its

analysis results for monotonic tension, stress relaxation, creep, and cyclic loadings agreed with test measurements.

Welding is used extensively in the manufacturing of heat exchangers. For many years in the power industry, welding has been successfully done on tubes, pipes, and plates made of the 9Cr-1MoVNb steel. However, in order to reduce the risk of cracking, restore ductility, and provide corrosion resistance; pre-weld and post-weld heat treatments are required as specified in Appendix D (Reference 12) and Article NB-4600 (Reference 13) of ASME Subsection III and ANSI/AWS D10.8 Standard (Reference 14). The non-mandatory preheat procedures given Appendix D of ASME Section III suggests a minimum preheat temperature of 204°C for the 9Cr-1MoVNb steel which has a P-No. of 5B. And with regard to the post-weld heat treatment (PWHT) of welds, Table NB-4622.1-1 in Subsection NB (applicable to components built per Subsection NH) provides mandatory requirements. Weldments of 9Cr-1MoVNb steel will require a holding temperature range of 677-760°C and minimum holding time of 30 min for thickness of 12.7 mm or less and 1 h per 25 mm for larger thicknesses up to 127 mm. Whereas, the ANSI/AWS standard recommends for 9Cr-1MoVNb steel a preheat minimum temperature of 200°C (to be maintained throughout the entire welding operation) and a post-weld heat treatment (tempering) consisting of heating the weldments to a temperature between 730 and 760°C. Some steel and component manufacturers (Reference 15) specify more controlled temperature range and longer holding time for PWHT of 9Cr-1MoVNB steel weldments. They recommend that the PWHT should be conducted at a minimum of 740°C with a target temperature of 760° and that the PWHT duration be always more than two hours even though the ASME code may allow shorter duration.

Various tests have demonstrated the importance of precise procedures for pre-weld and post-weld heat treatments. For instance, cracking of the 9Cr-1MoVNb steel weldments was observed (Reference 16) when no preheat was applied or when preheating was carried out at 93°C, whereas preheating to 204°C prevented cracking. Similarly, the study reported in Reference 17 showed clearly the effect of PWHT tempering temperature on the impact toughness of 9Cr-1MoVNb weldments. Tempering temperatures in the range of 450 to 610°C unexpectedly reduced the impact energy of the weldments compared to non heat treated samples. But the impact energy significantly improved with a tempering temperature of 750°C. The study also demonstrated the effect of tempering time on the impact energy. As the holding time was increased from 1 to 2 hours at 750°C, the impact energy increased from 31.4 to 57.8 J.

The 12Cr-2W steel was developed by Sumitomo Metal Industries Ltd. of Japan for use in power industry to attain higher service temperatures. The steel which is characterized by higher allowable stress and lower steam oxidation at elevated temperature compared to the 9Cr-1MoVNb has the added benefit of lower coefficient of thermal expansion which leads to lower thermal induced strains. The steel in its normalized and tempered condition is currently permitted in accordance with ASME B&PV Code Case 2180-2 (Reference 18) for use in components designed per Section I and Section VIII, Division 1 of the code. As mentioned earlier, some additional data have been obtained from the steel

manufacturer (see Reference 7), but in order for this steel to be used in nuclear heat exchanger construction it has to go through a long and systematic testing and qualification process.

In the following list of material properties, the remark 'has not yet been addressed' indicates that some information about the property is available in literature but the property was not addressed because of the limited funding in this preliminary phase of the project. The remark 'need to be developed' indicates that information about the property was not found in literature or in steel manufacturer's publications; as a result, material testing is required (see Section 4.1). When Reference 3 is shown as the source for a property of 9Cr-1MoVNb steel, this means that the property will be provided in the 2004 Edition of Subsection NH of the ASME Code.

3.1 12Cr-2W Steel

a. *Chemical Composition*: References 18 through 20.

b. *Thermal conductivity*: References 7 and 21, see Figure 6.

c. *Coefficient of linear Expansion:* References 7 and 21, see Figure 4.

d. *Specific Heat:* Reference 7.

e. *Modulus of Elasticity:* Reference 7, see Figure5.

f. *Heat treatment:* Reference 18.

g. *Tensile properties*: References 18, 19, 22, and 23.

h. *Allowable stress:* Reference 18, see Figure 3.

i. *Fatigue correlation:* Need to be developed.

j. *Allowable limits per ASME Subsection NH*: Need to be developed.

k. *Constitutive equations:* Need to be developed.

l. *Creep equation:* Need to be developed.

m. *Brittle fracture:* References 22 through 24.

n. *Weldments:* Have not yet been addressed.

o. *Corrosion / Oxidation in Steam:* References 7 and 23.

p. *Irradiation effect*: Has not yet been addressed.

q. *Thermal Aging:* Has not yet been addressed.

3.2 9Cr-1MoVNb Steel

a. *Chemical Composition*: References 5, 9, 19, and 25.

b. *Thermal conductivity*: References 5 and 25, see Figure 6.

c. *Coefficient of linear Expansion:* References 5 and 25, see Figure 4.

d. *Specific Heat:* Reference 5.

e. *Modulus of Elasticity:* References 5 and 25, see Figure 5.

f. *Heat treatment:* Reference 9.

g. *Tensile properties*: References 9 and 20.

h. *Allowable stress:* References 3 and 21, see Figure 3.

i. *Fatigue correlation*: References 3 and 5.

j. *Allowable limits per ASME Subsection NH*: Reference 3.

k. *Constitutive equations:* Need to be developed.

l. *Creep equation:* Reference 26.

m. *Brittle fracture:* References 5 and 24.

n. *Weldments:* Have not yet been addressed.

o. *Corrosion / Oxidation in Steam*: References 5, 7, 9, and 23.

p. *Irradiation effect*: Has not yet been addressed.

q. *Thermal Aging:* Has not yet been addressed.

4.0 RECOMMENDED FOLLOW UP STEPS

The preliminary phase of this project has been funded by the LDRD program. The results of the preliminary phase highlighted the importance of having a simplified and reliable means to quantify the cost advantages of the recently developed high strength and heat resistant ferritic steels with 9 to 13% chromium along with a complete database for these steels. In order for the project to achieve fully this goal, the following tasks are proposed.

4.1 Extending Material Database

The database and the simplified heat exchanger calculations are to be expanded to include the 9Cr-2W steel in addition to the 12Cr-2W and 9Cr-1MoVNb steels. The 9Cr-2W steel is a third generation ferritic steel, similar to the 12Cr-2W, and when it is in tube form it is referred to in ASTM Standards as T92. The database will also be expanded to cover the properties that have not been addressed in the preliminary phase for all the selected steels and will be organized in a convenient hypertext format.

Elevated temperature mechanical tests (cyclic mechanical and thermal loadings with different hold periods) are to be performed on the 12Cr-2W steel at 480 to 650°C. These tests which will be the first of its kind to be done on this steel are similar (but at a much smaller scale) to the tests done years ago at ORNL on the 9Cr-1MoVNb steel. It will be extremely useful to find out how the creep-fatigue interaction of 12Cr-2W compares with that of the 9Cr-1MoVNb. According to an advanced copy of the 2004 Edition of the ASME Subsection NH, the creep-fatigue interaction of the 9Cr-1MoVNb is rather restrictive (bilinear envelope has intersection at D_f = 0.10 and D_c = 0.01). If a more advanced ferritic steel such as the 12Cr-2W steel has a less restrictive creep-fatigue damage envelope, this would be advantageous for nuclear heat exchanger designs.

4.2 Extending Computer Program Capability

The computer program is to be extended to include the following calculations:

1. For a new material identifier (IMAT = 4), the program performs the calculations with the properties of the 9Cr-2W steel.

2. The program estimates the amount of corrosion on the steam side of the tube based on available test data and HX operating condition.

3. The program determines the pressure drop on the steam side.

4. The thermal model includes: (i) a film boiling region and (ii) temperature and pressure dependent thermal and physical properties.

5. The program estimates the inside diameter of the steam generator shell based on the number of tubes and tube outside diameter, pitch, and pattern. This will enable the assessment of the advanced material effect in reducing the shell weight in addition to the tube bundle weight.

6. The program performs the same calculations for an intermediate heat exchanger with liquid sodium on both the tube and shell sides.

4.3 Calculations with Advanced Ferritic Steels

After the new features are introduced in the computer program, the calculations are to be done for the following steam generator design conditions with the tube and shell made of 2¼Cr-1Mo steel (reference material), 12Cr-2W, 9Cr-1MoVNb, or 9Cr-2W:

AFR-300 Base Case

The steam generator design used for the AFR-300 plant study (see Reference 27) was a shell-and-tube, counter-flow, with the water/steam on the tube side. The tubes were straight double-walled tubes fabricated from 2¼Cr-1Mo steel and the steam outlet temperature was 457°C.

Higher Temperature Case

For the purpose of demonstrating clearly the advantages of high-strength and heat- resistant steels, a case similar to the AFR-300 design will be calculated with a steam outlet temperature of 538°C, instead of 457°C.

REFERENCES

1. Y. Shimakawa et al., "An Innovative Concept of a Sodium-Cooled Reactor to Pursue High Economic Competitiveness," Nuclear Technology, Volume 140, pp. 1-17, October 2002.

2. ASME Boiler & Pressure Vessel Code, Section III, Division 1, Subsection NH - Class 1 Nuclear Power Plant Components in Elevated Temperature Service, 2001 Edition, July 2001.

3. C.A. Sonna, ASME B&PV Subcommittee on Nuclear Power, Private Communication, December 2003.

4. J.S. McDonald, A. Andonedis, J. Matte III, Atomics International / Burns and Roe / ERDA-EPRI, Unpublished information, May 1977.

5. Material Data for Advanced Accelerator Applications, Unpublished information, January 2003.

6. R. Viswanathan and W.T. Bakker, "Materials for Boiler in Ultra Supercritical Power Plants," Proceedings of 2000 International Joint Power Generation Conference, IJPGC2000-15049, American Society of Mechanical Engineers, pp. 1-22, July 2000.

7. Proprietary Data from Sumitomo Metal Industries, Ltd. of Japan, Permission to use data in an ANL publication was obtained, April 2004.

8. R.W. Swindeman, “Cyclic Stress-Strain-Time Response of a 9Cr-1Mo-V-Nb Pressure Vessel Steel at High Temperature,” ASTM STP 942, pp. 107-122, 1987.

9. J.R. DiStefano et al., Oak Ridge National Laboratory, Unpublished information, October 1986.

10. M. Yaguchi and Y. Takahashi, “Unified Inelastic Constitutive Model for Modified 9Cr-1Mo Steel Incorporating Dynamic Strain Aging Effect,” JSME International Journal (in Japanese), Series A, Vol. 42, No. 1, pp. 1-10, January 1999.

11. M. Yaguchi and Y. Takahashi, “Modeling of Temperature Dependence of Ratcheting Deformation Behavior of Modified 9Cr-1Mo Steel,” Journal of the Society of Materials Science (in Japanese), Vol. 51, No. 3, pp. 299-306, March 2002.

12. ASME Boiler & Pressure Vessel Code, Section III , Division 1, Appendices, 2001 Edition, July 2001.

13. ASME Boiler & Pressure Vessel Code, Section III , Division 1, Subsection NB – Class 1 Components, 2001 Edition, July 2001.

14. “Recommended Practices for Welding of Chromium-Molybdenum Steel Piping and Tubing,” ANSI/AWS D10.8-96, American Welding Society, July 17, 1996.

15. Y. Tsuchida, K.Tokuno, and K. Hashimoto, “Development and BOF Manufacture of Modified 9Cr-1Mo Steel Plates with Excellent Strength and Toughness,” Nippon Steel Technical Report No. 58, pp. 27-35, July 1993.

16. R.L. Klueh and D.R. Harries, “High-Chromium Ferritic and Martensitic Steels for Nuclear Applications,” ASTM Publication Number MONO3, 2001.

17. R.K. Shiue, K.C. Lan, and C. Chen, “Toughness and Austenite Stability of Modified 9Cr-1Mo Welds after Tempering,” Materials Science and Engineering, Vol. A287, pp. 10-16, 2000.

18. “Seamless 12Cr-2W Material for Sections and I and VIII, Division 1,” Code Case 2180-2, ASME Boiler and Pressure Vessel Code, American Society of Mechanical Engineers, 2001 Edition.

19. “Standard Specification for Seamless Ferritic and Austenitic Alloy-Steel Boiler, Superheater, and Heat-Exchanger Tubes,” ASTM Standard A 213, ASTM International, 2004 Edition.

20. A. Iseda, “Advanced Heat Resistant Steel Tubes and Pipes for Power Generation Boilers,” CEPSI 2002, Proceedings of the 14th Conference of the Electric Power Supply Industry, pp. 350-355, November 2002.

21. ASME Boiler and Pressure Vessel Code, Section II, Part D - Properties, American Society of Mechanical Engineers, 2001 Edition.

22. A. Iseda et al., "Development of a New 0.1C-11Cr-2W-0.4Mo-1Cu Steel for Large Diameter and Thick Wall Pipe for Boilers," Proceedings of the 5th International Conference on Creep of Materials, pp. 389-397, May 1992.

23. Y. Sawaragi, et al., "Development of a High Strength 12Cr Steel (HCM12A) Tubes and Pipes for Boilers," Proceedings of the 1994 Conference on Materials for Advanced Power Engineering, Volume 1, pp. 309-318, 1994.

24. M.G. Horsten, E.V. van Osch, D.S. Gelles, and M.L. Hamilton, "Irradiation Behavior of Ferritic-Martensitic 9-12Cr Steels," Effects of Irradiation on Materials: 19th International Symposium, ASTM STP 1366, pp. 579- 593, 2000.

25. V.K. Sikka and P. Patriarca, Oak Ridge National Laboratory, Unpublished information, December 1983.

26. R.W. Swindeman, "Construction of Isochronous Stress-Strain Curves for 9Cr-1Mo-V Steel," PVP-Volume 391, Advances in Life Prediction Methodology, American Society of Mechanical Engineers, pp. 95-100, August 1999.

27. C.W. Grandy et al., Argonne National Laboratory, Unpublished information, October 2002.

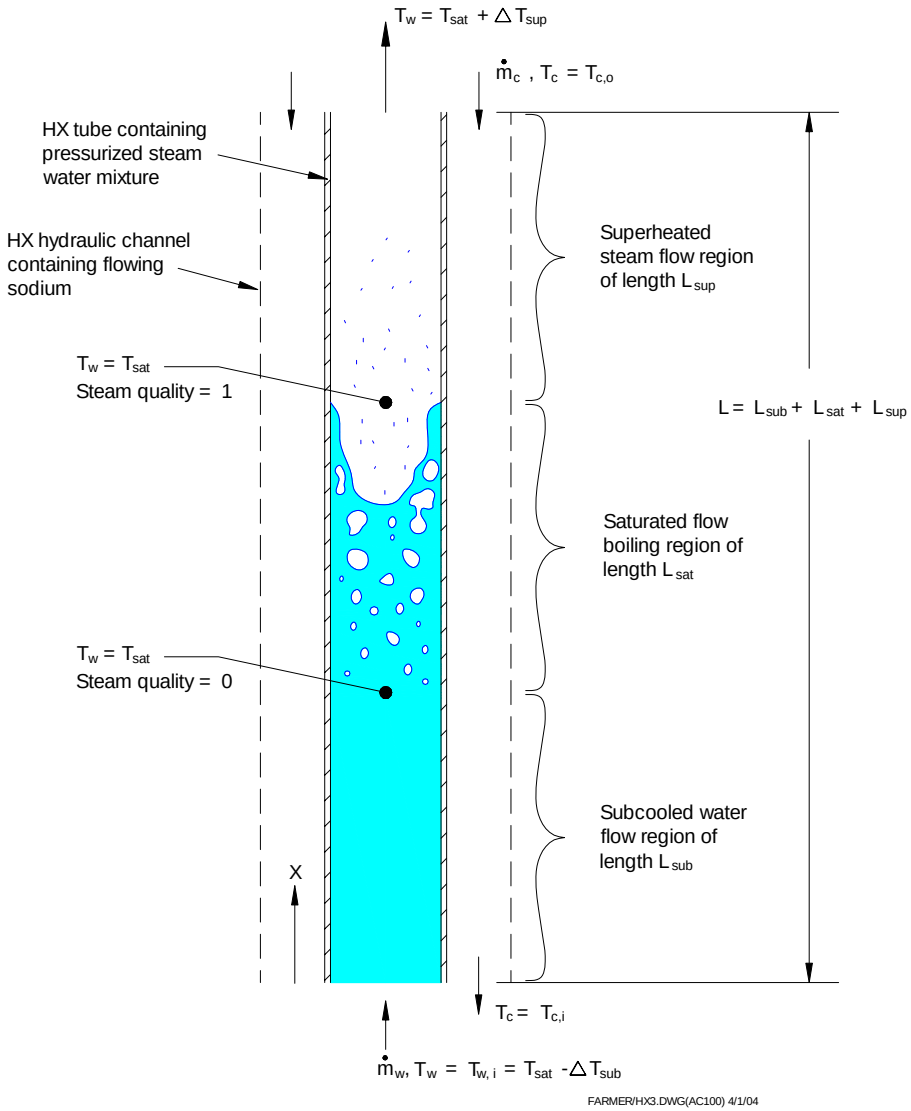

Figure 1. Modeling of Water/Steam Flow through Tube in Superheater Steam Generator.

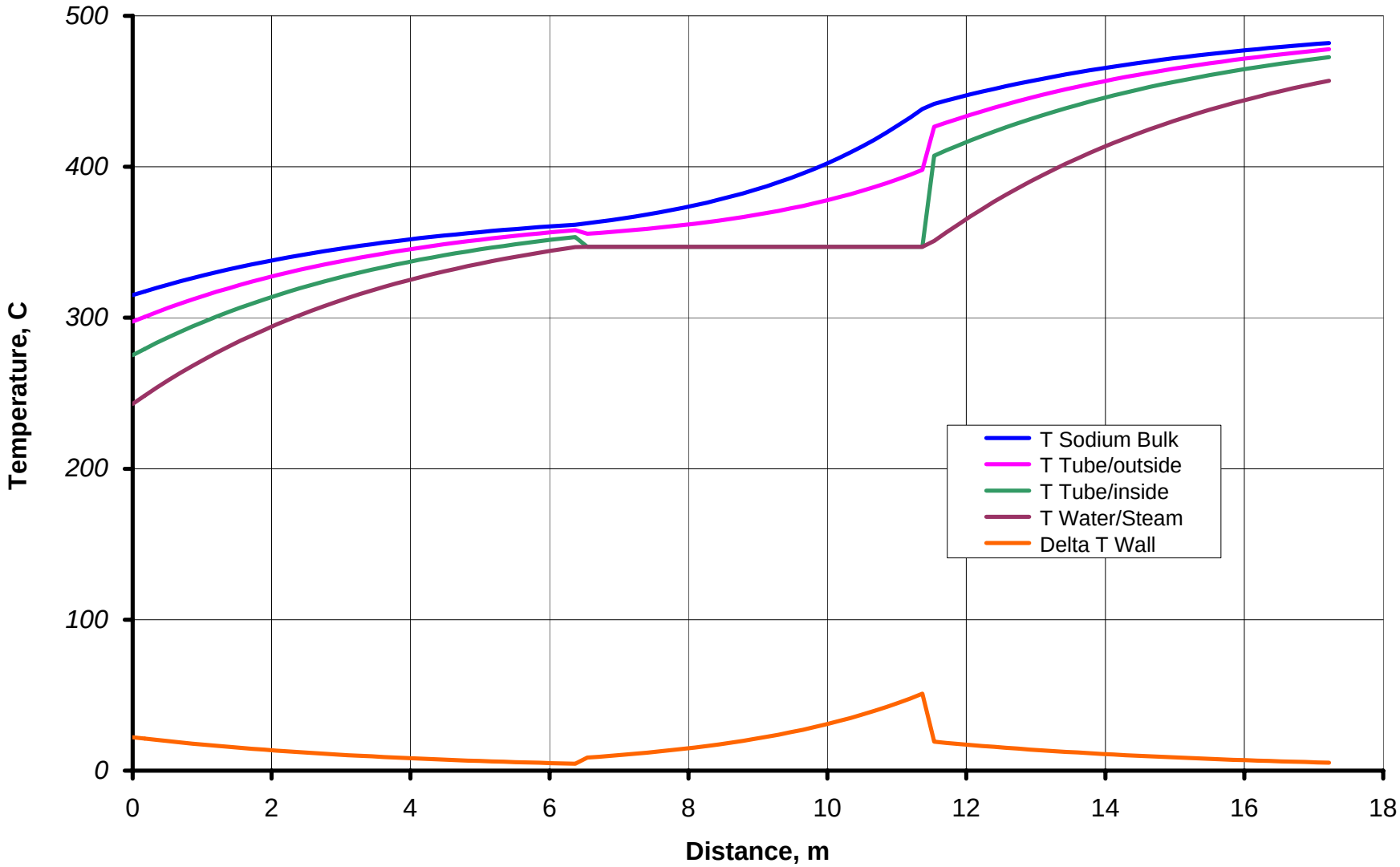

Figure 2. Temperature Distributions along a Steam Generator Tube Made of 2.25Cr-1Mo Steel.

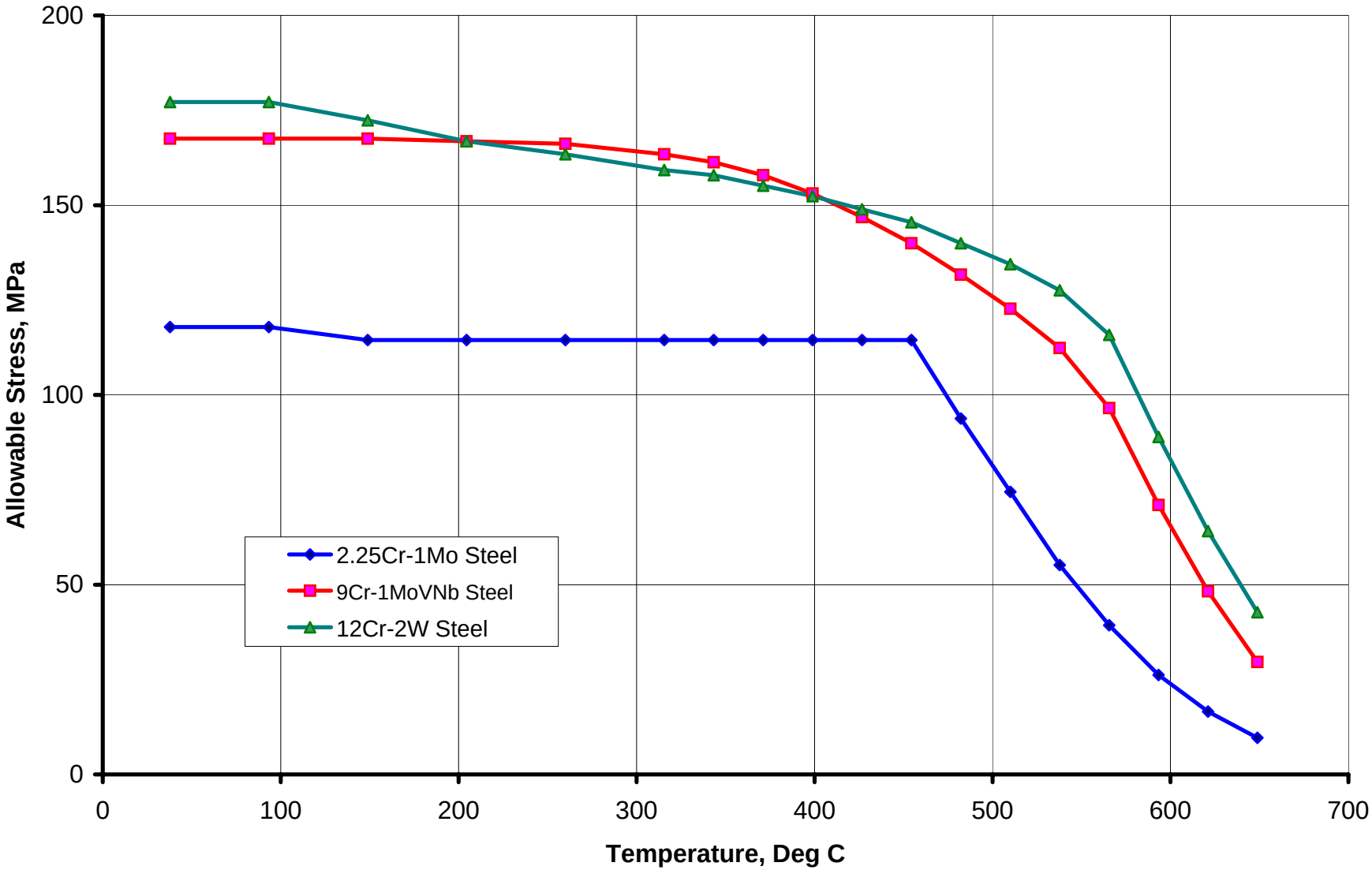

Figure 3. Allowable Stresses of 2.25Cr-1Mo, 9Cr-1MoVNb, and 12Cr-2W Steels.

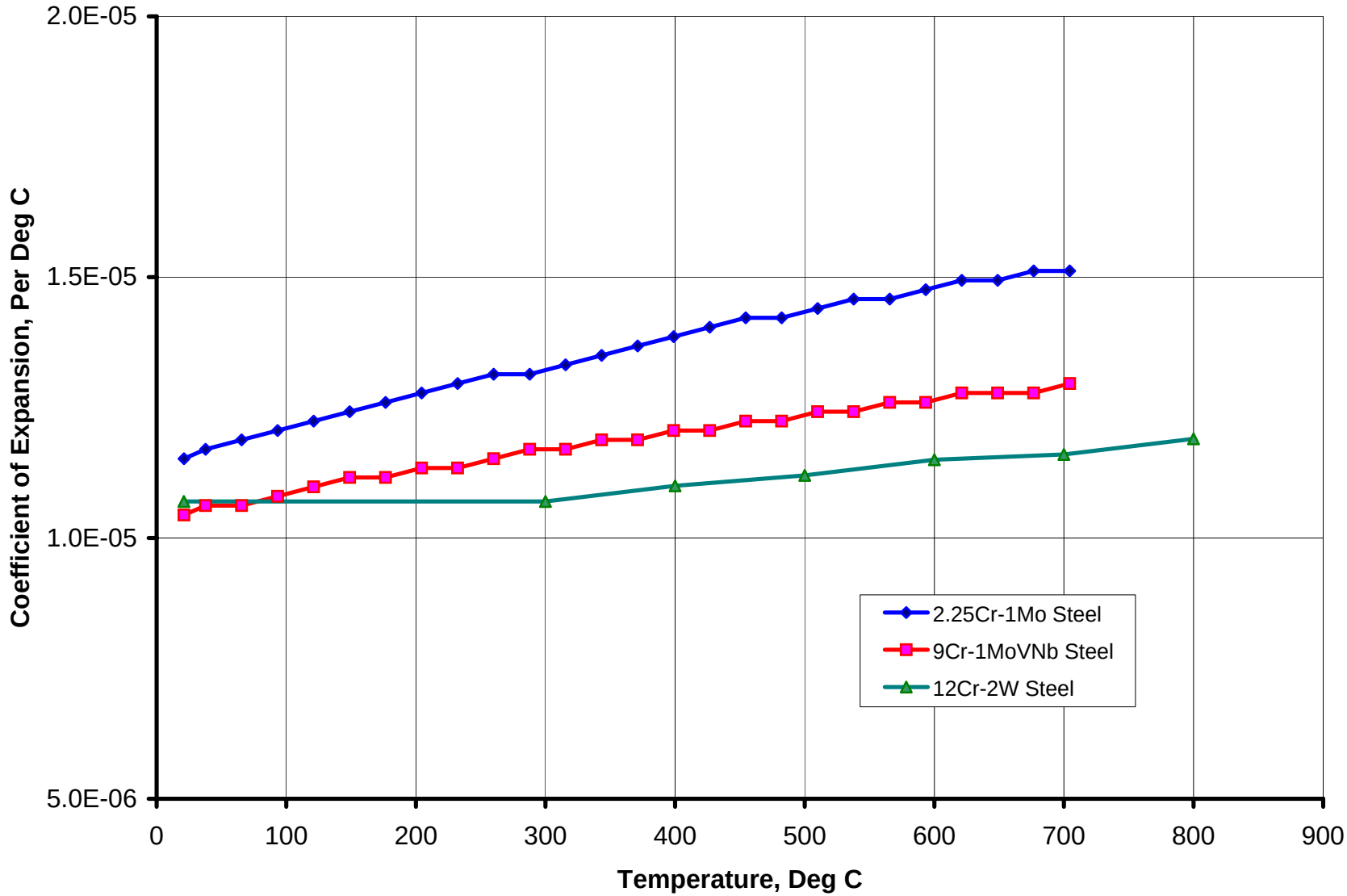

Figure 4. Coefficient of Thermal Expansion of 2.25Cr-1Mo, 9Cr-1MoVNb, and 12Cr-2W Steels.

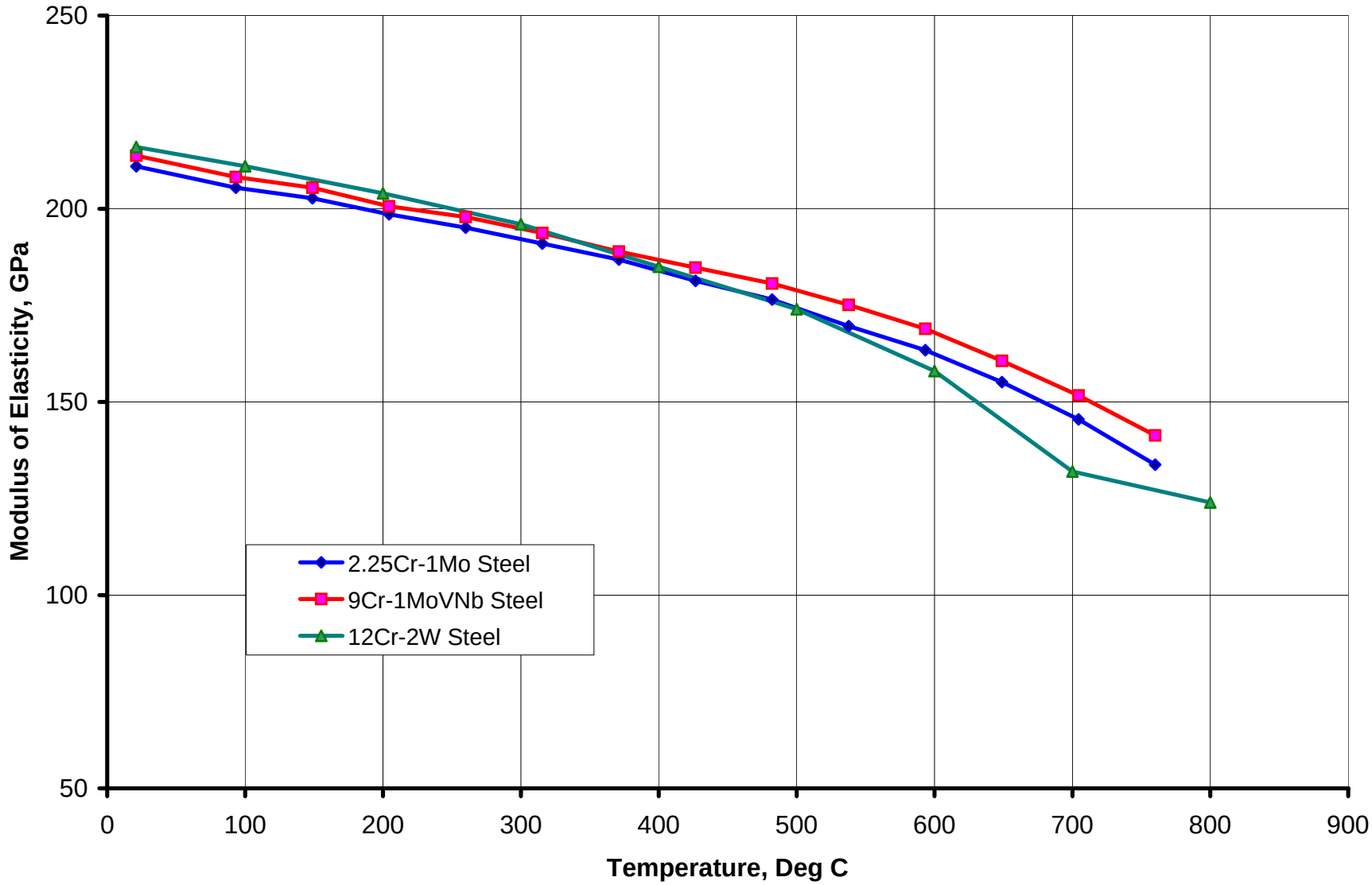

Figure 5. Modulus of Elasticity of 2.25Cr-1Mo, 9Cr-1MoVNb, and 12Cr-2W Steels.

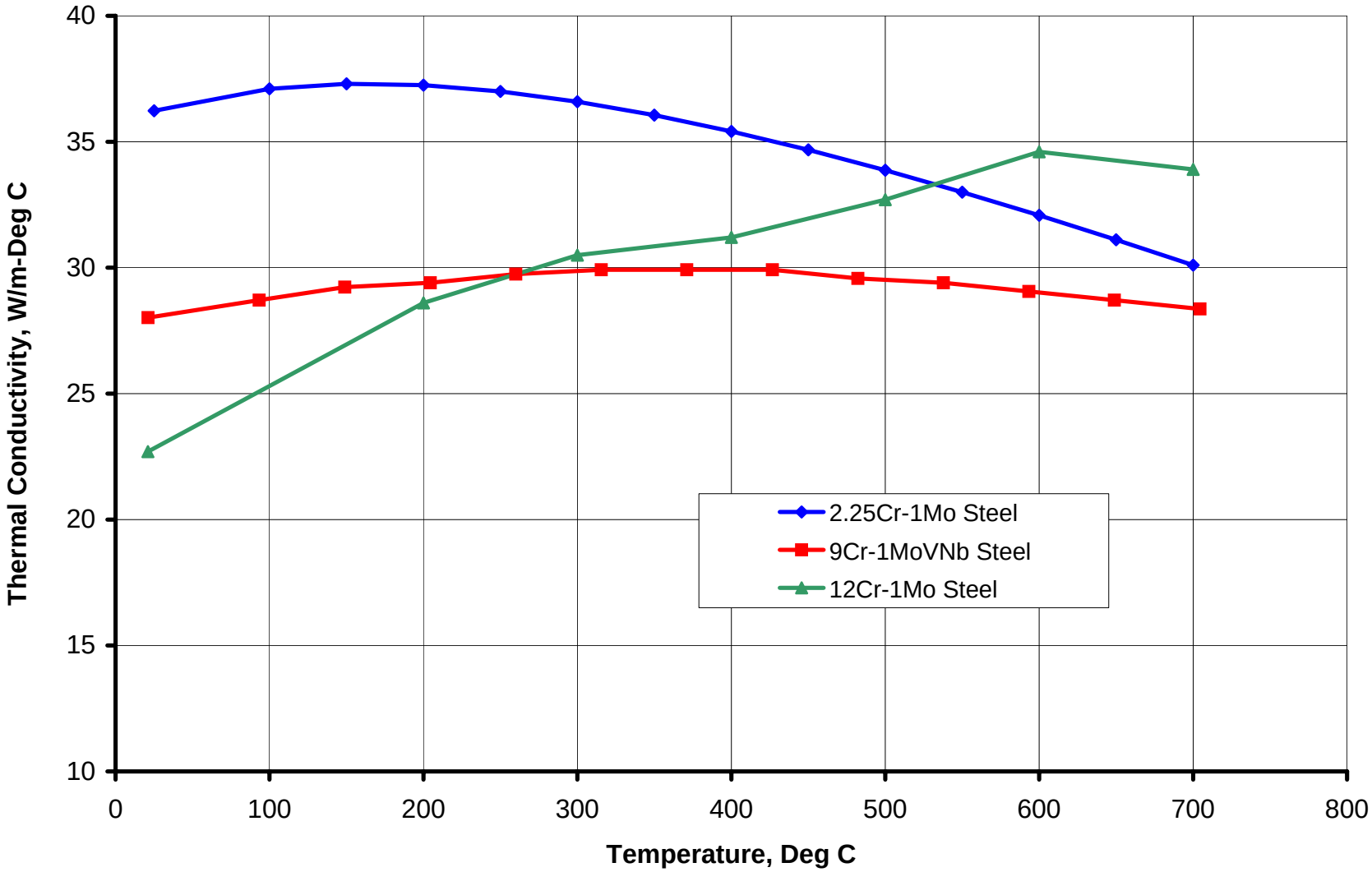

Figure 6. Thermal Conductivity of 2.25Cr-1Mo, 9Cr-1MoVNb, and 12Cr-2W Steels.

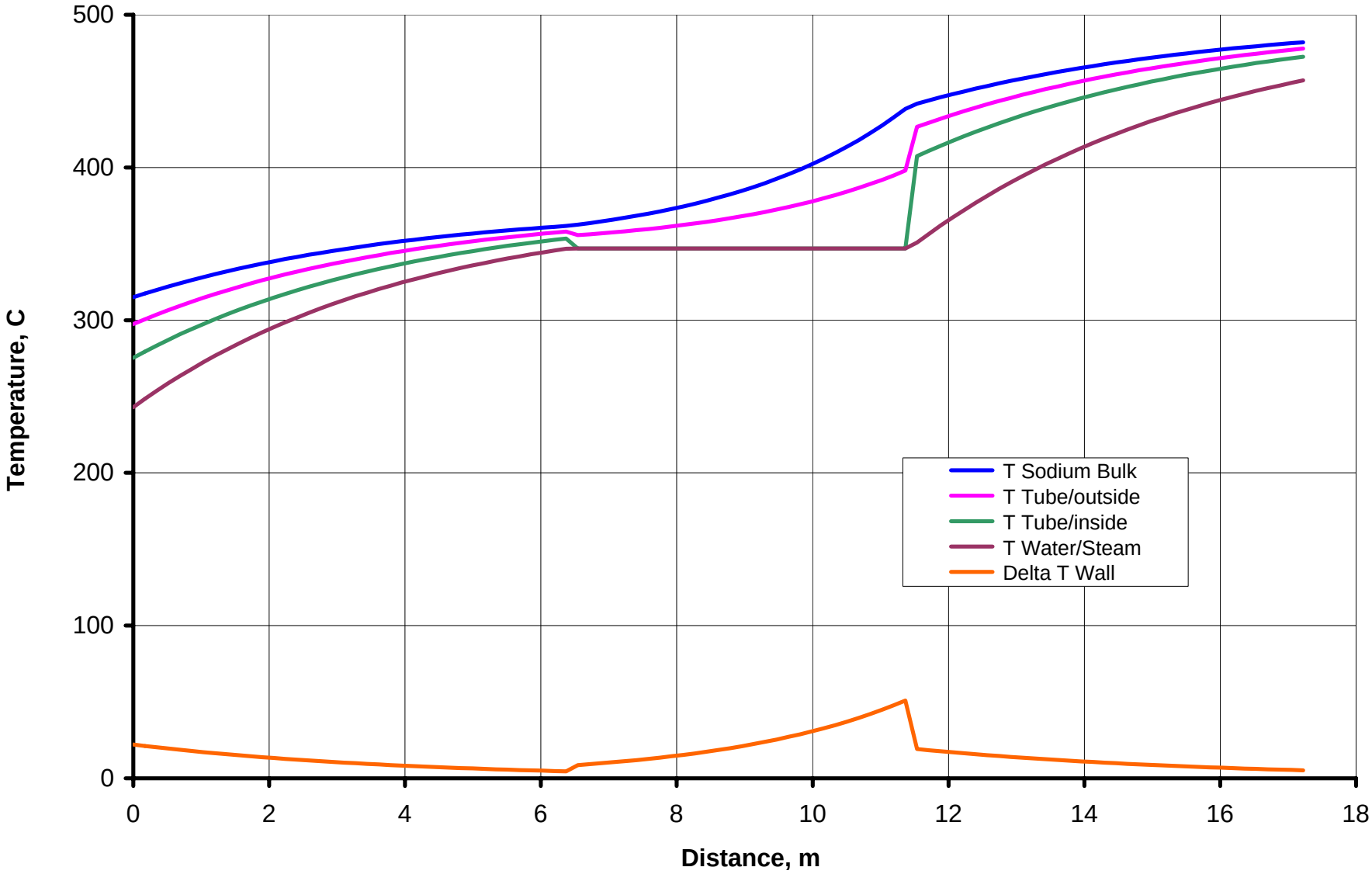

Figure 7. Temperature Distributions along a Steam Generator Tube Made of 9Cr-1MoVNb Steel.

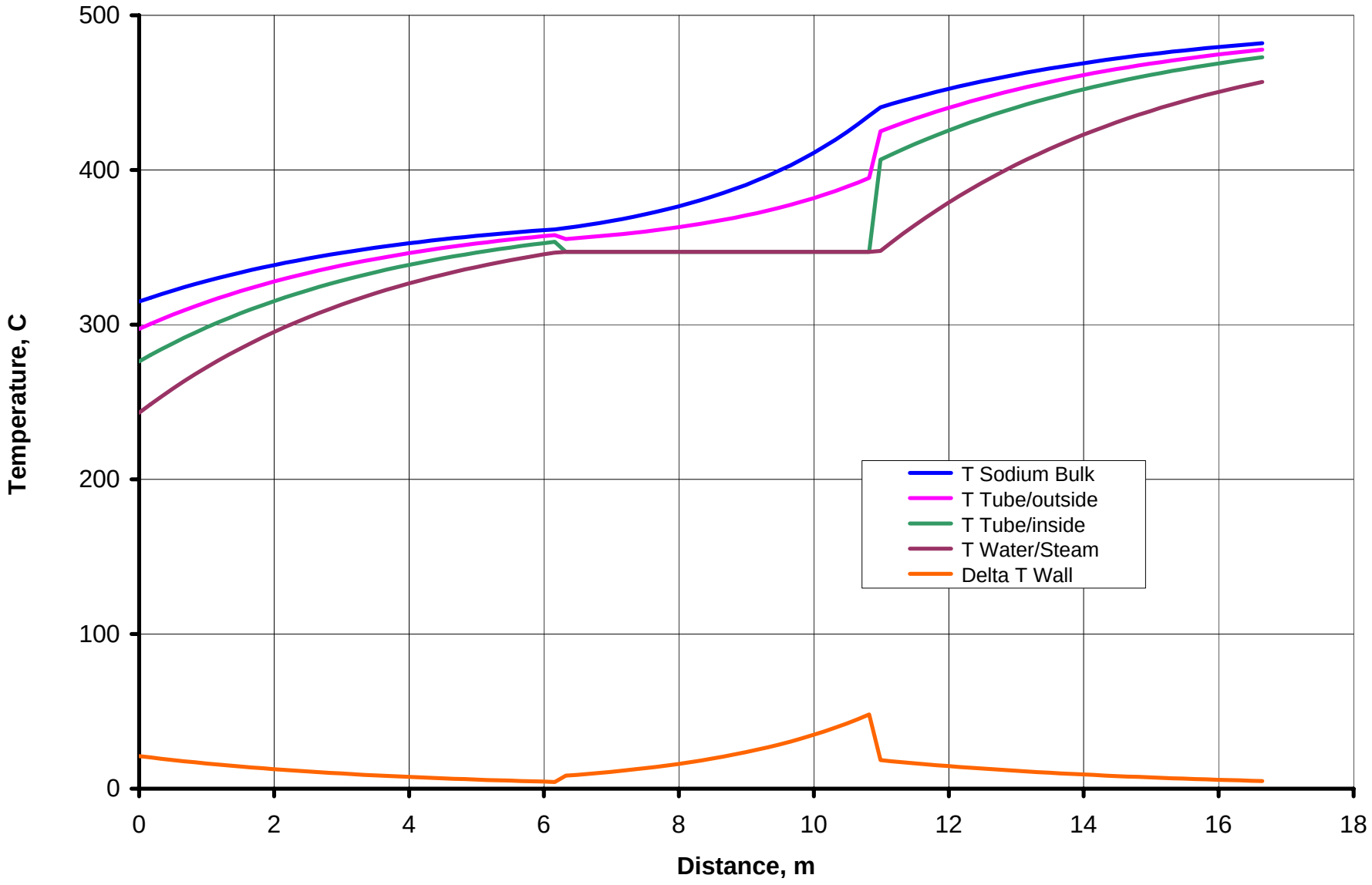

Figure 8. Temperature Distributions along a Steam Generator Tube Made of 12Cr-2W Steel.

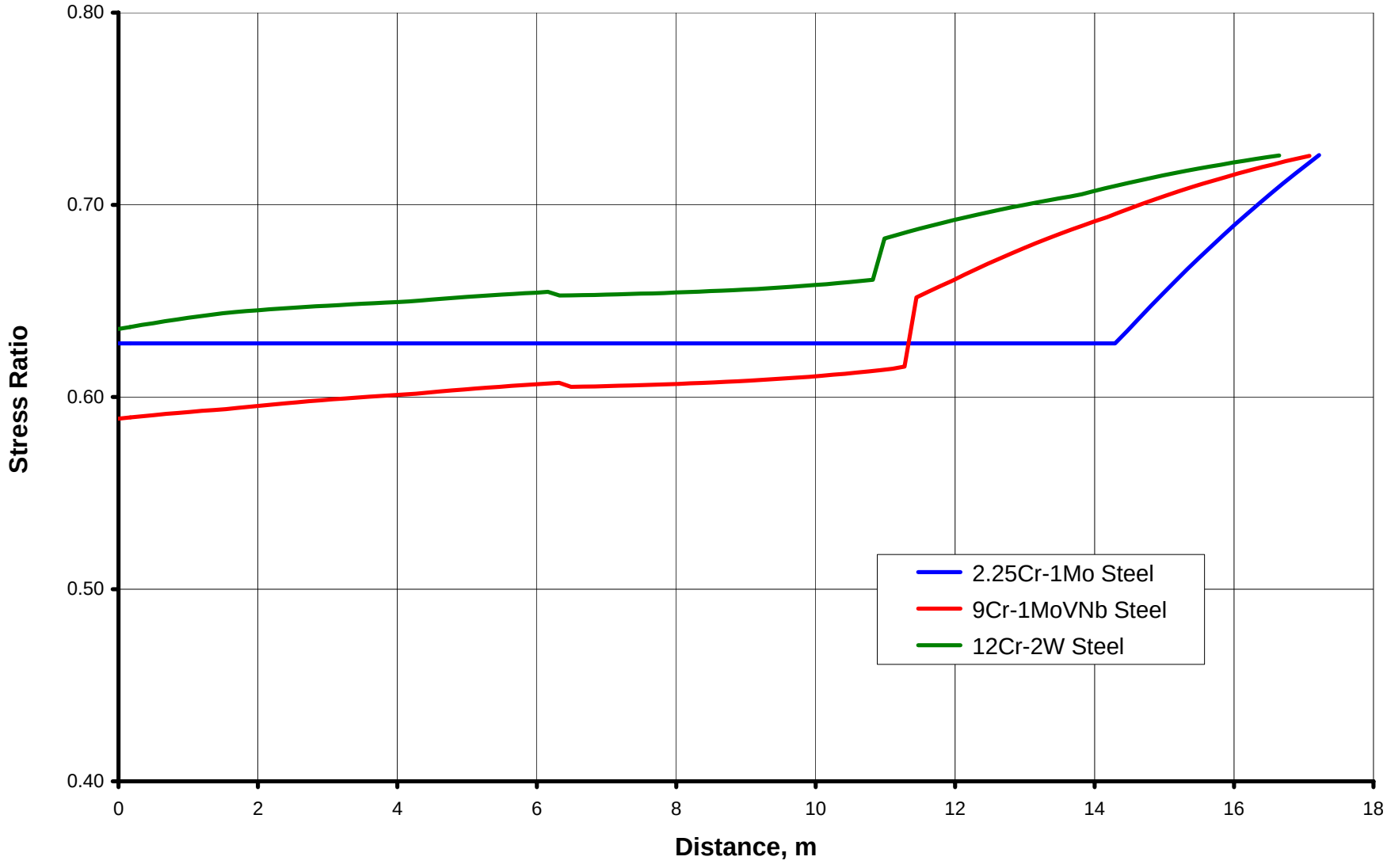

Figure 9. Ratio of Tube Stress due to Internal Pressure to Material Allowable Stress.

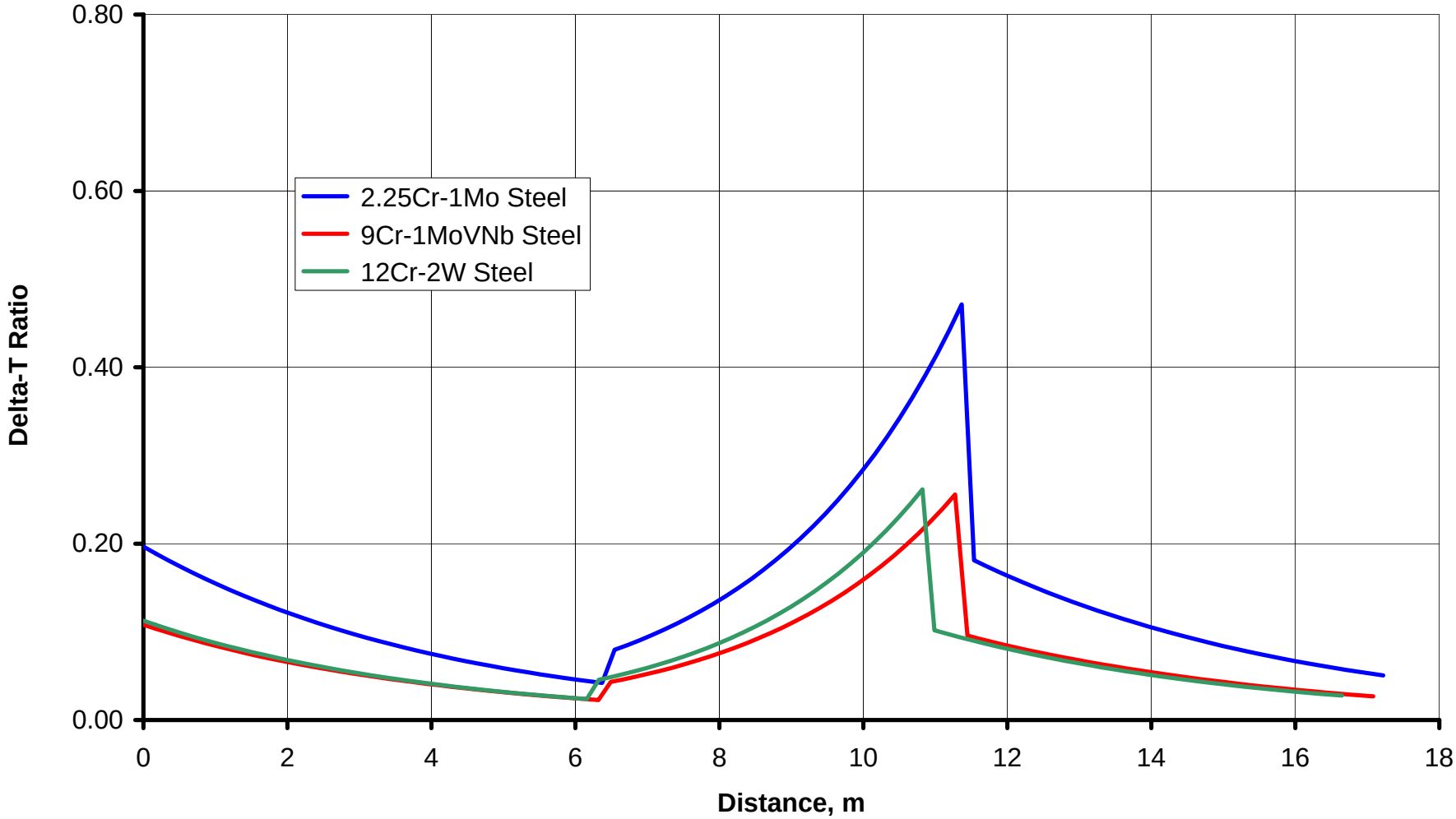

Figure 10. Ratio of Temperature Difference through Tube Wall to Material Fatigue Allowable Limit.

Table 1. Input Data Description of Computer Code HeatXchngr1

Line	Input Variables	Variable Definition	Units
1	TITLE	TITLE = 80-column description of case to be analyzed	
2	PHX	PHX = HX thermal power	W
3	THXOUT, THXIN	THXOUT = liquid metal outlet temperature THXIN = liquid metal inlet temperature	°C °C
4	DTUBE, DHYDRO, NTUBE	DTUBE = HX tube OD DHYDRO = hydraulic diameter of shell side NTUBE = number of tubes in HX	m m
5	TUBEWALL, TKWALL	TUBEWALL = HX tube wall thickness TKWALL = wall thermal conductivity	m W/m-°C
6	DENNA, VISNA, TKNA, CPNA	DENNA = sodium density VISNA = sodium dynamic viscosity TKNA = sodium thermal conductivity CPNA = sodium specific heat	kg/m^3 kg/m-s W/m-°C J/kg-°C
7	TSUB, TSUP	TSUB = HX feedwater inlet subcooling (>0) TSUP = HX steam outlet superheat (>0)	°C °C

Table 1. Input Data Description of Computer Code HeatXchngr1 (Continued)

Line	Input Variables	Variable Definition	Units
8	TSAT, ELIQ, HLV	FSAT = water saturation temperature at HX operating pressure ELIQ = liquid water specific enthalpy at saturation temperature HLV = water latent heat of vaporization	°C J/kg J/kg
9	DENH2O, VISHWO, TKH2O, CPH2O	DENH2O = water density VISH2O = water dynamic viscosity TKH2O = water thermal conductivity CPH2O = water specific heat	kg/m^3 kg/m-s W/m-°C J/kg-°C
10	DENSTEAM, VISSTEAM, TKSTEAM, CPSTEAM	DESNSTEAM = steam density VISSTEAM = steam dynamic viscosity TKSTEAM = steam thermal conductivity CPSTEAM = steam specific heat	kg/m^3 kg/m-s W/m-°C J/kg-°C
11	NPLOT, ICALC, IMAT, PRESS, CORROS	NPLOT = number of subintervals into which HX tube length is divided in order to print out the temperatures along the HX tube channel ICALC = calculation option for stress, strain, and weight (1: thermal calculations only, 2: stress, strain, and weight calculations with fixed tube dimensions) IMAT = tube material identifier, required only with ICALC > 1 (1: T22 steel, 2: T91 steel, 3: T122 steel) PRESS = steam pressure, required only with ICALC > 1 CORROS = tube wall corrosion allowance on the water/steam side, required only with ICALC > 1	 MPa m

Table 2. Comparison of Bench Mark Parameters and HX Model Results

SG Configuration		Counter Flow, Single Wall Water on Tube Side	
		Input Parameters	
		AI-SG Hockey Stick Design (Reference 4)	HX Model
Thermal Rating		292 MWt	
Na Temperature In		482 C (900 F)	
Na Temperature Out		315 C (600 F)	
Water Temperature In		243 C (470 F)	
Water Inlet Pressure		16.2 MPa (2350 psi)	16.0 MPa (2321 psi)
Steam Temperature Out		457 C (855 F)	
Steam Outlet Pressure		15.7 MPa (2275 psi)	16.0 MPa (2321 psi)
Tube OD		1.59 cm (0.625 in)	
Tube Wall Thickness		2.77 mm (0.109 in)	
Tube Pitch		2.87 cm (1.13 in)	
Number of Tubes		2200	
		Results	
Na Flow		1.36E+03 kg/s (10.8E+06 lb/hr)	1.37E+03 kg/s (10.9E+06 lb/hr)
Water/Steam Flow Rate		1.37E+02 kg/s (1.09E+06 lb/hr)	1.48E+02 kg/s (1.18E+06 lb/hr)
Active Heat Transfer Length		23.5 m (77.1 ft)	17.3 m (56.8 ft)

Table 3. Comparison of Input Parameters and Calculation Results for Steam Generator Tubes Made of 2.25Cr-1Mo, 9Cr-1MoVNb, or 12Cr-2W Steels

Design Parameter	**2.25Cr-1Mo Steel**	**9Cr-1MoVNb**	**12Cr-2W**
Input Parameters:			
SG thermal rating, MW	292		
Number of tubes	2200		
Steam pressure, MPa	16.0		
Tube OD, cm	1.590	1.480	1.464
Tube thickness, mm	2.77	2.22	2.14
Hydraulic diameter, cm	4.150	3.860	3.821
Corrosion allowance, mm	1.0		
Calculation Results:			
Tube length, m	17.22	17.08	16.65
Circumferential stress, MPa	71.86	97.05	102.56
Max stress ratio	0.7259	0.7255	0.7257
Max ΔT through wall, C	50.96	51.63	47.93
Max ΔT through wall ratio			
Actual	0.4713	0.2558	0.2615
Relative to 2.25Cr-1Mo	1.0	0.543	0.555
Differential thermal expansion between tube and shell			
Actual, mm	5.23	4.27	3.71
Relative to 2.25Cr-1Mo	1.0	0.816	0.710
Total tube weight			
Actual, kg	33,890	25,490	24,210
Relative to 2.25Cr-1Mo	1.0	0.752	0.714

APPENDIX A

THERMAL-HYDRAULIC MODEL FOR SHELL-AND-TUBE
SUPERHEATED STEAM GENERATOR

ARGONNE NATIONAL LABORATORY **INTRA-LABORATORY MEMO**

April 5, 2004
ED&A#70

TO: Sami Kamal NE

FROM: Mitch Farmer NE

SUBJECT: **Thermal-Hydraulics Model for Shell-and-Tube Type Superheated Steam Generator**

Reference: W.C. Grandy et al., Argonne National Laboratory, Unpublished information, October 2002.

Introduction

A simple thermal-hydraulics model of a classic counter-current flow, shell-and-tube type, superheated steam generator has been developed to support your efforts targeted at assessing different types of steels for use in advanced reactor HX design applications. In particular, for a given reactor core thermal power level and core inlet and exit temperatures, the model calculates the required HX tube length to achieve a specified steam superheat given the HX operating pressure, inlet feedwater subcooling, and mechanical design characteristics (i.e., the number of tubes, as well as the tube thermal conductivity, pitch, diameter, and wall thickness). The model also provides the bulk liquid metal (shell-side) temperature, bulk steam/water (tube-side) temperature, and the tube inner and outer surface temperatures as a function of distance along the entire HX tube length. The tube wall temperature profile is the key piece of information needed to assess materials issues related to the HX design.

This memo begins by providing a summary description of the HX thermal-hydraulics model. The model description is followed by a sample application to the AFR-300. A simple computational tool was also developed to facilitate application of the model to various HX designs. That tool (coded in Fortran) was transmitted to you under separate cover.

Summary Model Description

A depiction of the physical situation is provided in Figure 1. The modeling considers a single hydraulic sub-channel for a counter-current flow, shell-and-tube type, superheated steam generator that is vertically oriented. The water flow is through the tube side of the HX while the liquid metal flows through the shell side. The model assumes that the tube side is maintained at a uniform pressure which fixes the boiling point at the corresponding saturation temperature for

the HX pressure. The model is strictly thermodynamic; i.e., the pressure drop across the HX due to flow and form-frictional losses are not evaluated as part of this work.

As shown in Figure 1, for each sub-channel of the HX, the feedwater is assumed to enter the tube from below at a specified subcooling relative to the saturation temperature. As the water flows through the channel, it is first heated by forced convection single-phase heat transfer to near the saturation temperature. Once the boiling point is reached, a two-phase boiling heat transfer region occurs in which the liquid-component of the steam/water mixture is steadily vaporized and the steam quality eventually reaches unity. Finally, another single phase flow region is encountered where the steam undergoes additional heating to a specified superheat relative to the saturation point at the HX exit. Individual models for each of these three flow regions are developed below. However, simple expressions are first developed that relate the sub-channel liquid metal and feedwater flowrates to the specified HX power level, as well as the specific enthalpy change of the water coolant as it flows through the HX.

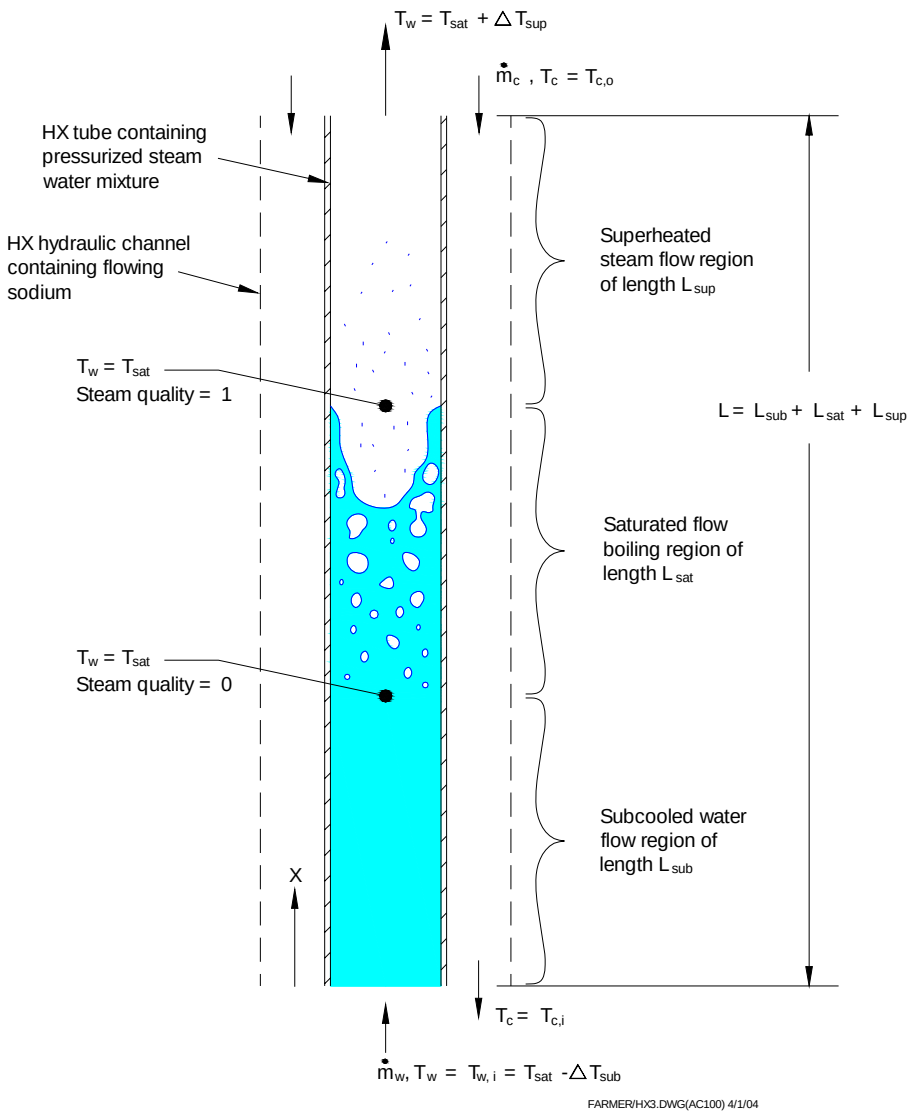

Figure 1. Depiction of water flow through a tube in a superheated steam generator.

For a given core (or HX) thermal power level and inlet and exit temperatures, the required liquid metal mass flowrate to remove the thermal energy is given through the equation:

$$\dot{m}_{core} = \frac{P_{core}}{c_c \Delta T_{core}} = \frac{P_{core}}{c_c (T_{c,o} - T_{c,i})} \tag{1}$$

where:

P_{core}	=	core (or HX) thermal power level,
c_c	=	liquid metal specific heat,
$T_{c,o}$	=	core exit temperature (or HX inlet temperature),
$T_{c,i}$	=	core inlet temperature (or HX exit temperature), and
ΔT_{core}	=	temperature rise across the core (or temperature reduction across the HX).

Neglecting any metal flow bypass for the HX, then the corresponding single-channel metal flowrate for a given number of HX tubes is thus:

$$\dot{m}_c = \frac{\dot{m}_{core}}{N_T} = \frac{P_{core}}{c_c (T_{c,o} - T_{c,i}) N_T} \tag{2}$$

where:

N_T = number of tubes in the HX.

In order to determine the feedwater flowrate to the HX, the specific enthalpy change of the coolant across the HX must be specified. The specific enthalpy of the coolant at the inlet and exits to the HX are defined as:

$$\begin{aligned} e_{w,i} &= e_{liq} - c_w \Delta T_{sub} \\ e_{w,o} &= e_{liq} + e_{lv} + c_v \Delta T_{\sup} \end{aligned} \tag{3}$$

where:

e_{liq}	=	liquid phase specific enthalpy at the saturation point,
c_w	=	liquid phase specific heat,
e_{lv}	=	latent heat of vaporization,
c_v	=	vapor phase specific heat,
ΔT_{sup}	=	vapor (steam) superheat at HX exit, and
ΔT_{sub}	=	feedwater subcooling at HX inlet.

Thus, the specific enthalpy change of the coolant across the HX is given by:

$$\Delta e_w = e_{w,o} - e_{w,i} = c_w \Delta T_{sub} + e_{lv} + c_v \Delta T_{\sup} \tag{4}$$

The required feedwater flowrate to the HX to achieve thermodynamic equilibrium with the core thermal power is thus:

$$\dot{m}_{w,HX} = \frac{P_{core}}{\Delta e_w} \tag{5}$$

Finally, the corresponding single-channel water flowrate for a given number of HX tubes is given by:

$$\dot{m}_w = \frac{\dot{m}_{w,HX}}{N_T} = \frac{P_{core}}{N_T \Delta e_w} \tag{6}$$

This completes the specification of the sub-channel liquid metal and feedwater flowrates in terms of core thermal power level, number of HX tubes, and the channel inlet and exit temperatures. Thermodynamic models for each of the three heat transfer regions in the flow channel are now developed.

Inlet Subcooling Region

The coordinate system and nomenclature for this phase of the modeling are shown in Figures 1 and 2. An energy balance on the tube side of the channel yields the following differential equation governing the temperature evolution of the subcooled water:

$$\dot{m}_w c_w \frac{dT_w}{dx} = 2\pi R_{T,i} h_w (T_{b,w} - T_w) \tag{7}$$

where:

$R_{T,i}$	=	HX tube inner radius,
h_w	=	convective heat transfer coefficient from water to the tube wall, and
$T_{b,w}$	=	temperature at the inner surface of the tube wall.

Correlations for the convective heat transfer coefficients used in this work are provided later in this section. Equation 7 is subject to the initial condition:

$$T_w\big|_{x=0} = T_{w,i} = T_{sat} - \Delta T_{sub} \tag{8}$$

where:

T_{sat}	=	water saturation temperature at HX operating pressure, and
$T_{w,i}$	=	feedwater temperature at the HX inlet.

Similarly, the differential equation governing the temperature evolution of the liquid metal in the subcooled region is deduced as:

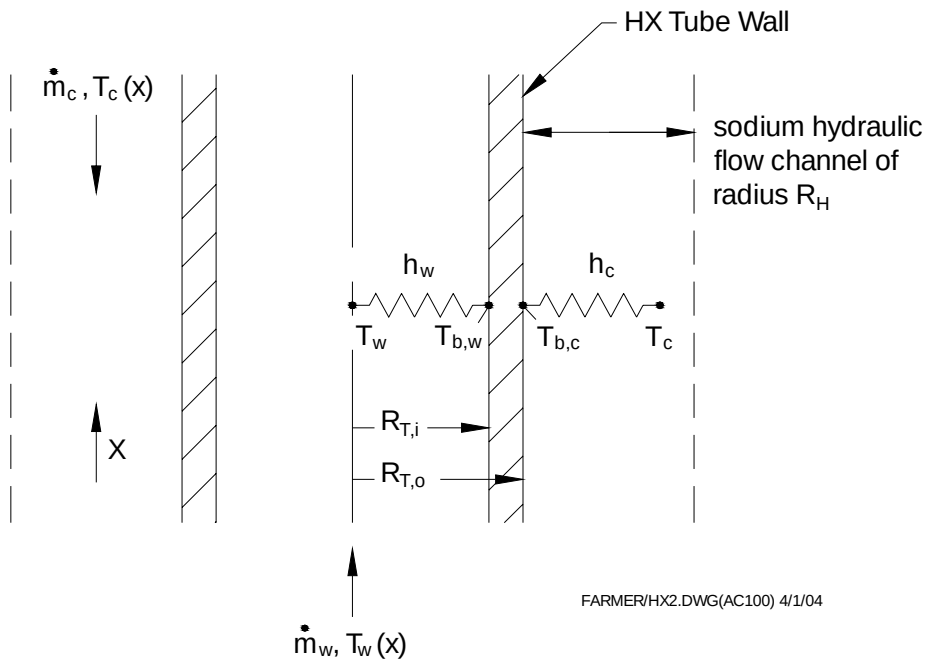

Figure 2. Depiction of geometry and nomenclature for inlet flow subcooling region.

$$\dot{m}_c\, c_c \frac{dT_c}{dx} = 2\pi R_{T,o} h_c (T_{b,c} - T_c) \tag{9}$$

where:

$R_{T,o}$	=	HX tube outer radius = $R_{T,i} + t_w$,
t_w	=	tube wall thickness,
h_c	=	convective heat transfer coefficient from liquid metal to the tube wall, and
$T_{b,c}$	=	temperature at the outer surface of the tube wall.

This equation is subject to the initial condition:

$$T_c\big|_{x=0} = T_{c,i} \tag{10}$$

For the purposes of integrating Eqs. 7 and 9, the tube surface inner and outer surface temperatures can be eliminated in terms of the bulk water and liquid metal temperatures by requiring continuity of the heat flux across the tube wall. Assuming steady-state heat transfer conditions and accounting for the effects of curvature on conduction through the wall, then the energy balances at the tube wall inner and outer surfaces are, respectively,

$$\frac{k(T_{b,c} - T_{b,w})}{R_{T,i} \ln(R_{T,o} / R_{T,i})} = h_w (T_{b,w} - T_w) \tag{11}$$

$$h_c(T_c - T_{b,c}) = \frac{k(T_{b,c} - T_{b,w})}{R_{T,o}\ln(R_{T,o}/R_{T,i})} \tag{12}$$

where:

k = HX tube wall thermal conductivity.

With these two expressions, the following two simultaneous differential equations governing the evolution of the bulk liquid metal and water temperatures in the inlet subcooling region are obtained:

$$\frac{dT_w}{dx} = \alpha_{sub}(T_c - T_w) \tag{13}$$

$$\frac{dT_c}{dx} = \beta_{sub}(T_c - T_w) \tag{14}$$

where:

$$\alpha_{sub} = \frac{2\pi\xi_{sub}}{\dot{m}_w c_w} \tag{15}$$

$$\beta_{sub} = \frac{2\pi\xi_{sub}}{\dot{m}_c c_c} \tag{16}$$

$$\xi_{sub} = \frac{h_c}{R_{T,i}} + \frac{h_w}{R_{T,o}} + \frac{h_c h_w}{k}\ln(R_{T,o}/R_{T,i}) \tag{17}$$

Integration of Eqs. 13-14 subject to the initial conditions given by Eqs. 8 and 10 yields the following solutions for the bulk water and liquid metal temperatures in the subcooled inlet region:

$$T_w = \begin{cases} T_{w,i} + \alpha_{sub}(T_{c,i} - T_{w,i})x, & \alpha_{sub} = \beta_{sub} \\ T_{w,i} + \left(\dfrac{\alpha_{sub}}{\alpha_{sub} - \beta_{sub}}\right)(T_{c,i} - T_{w,i})(1 - e^{(\beta_{sub} - \alpha_{sub})x}), & \alpha_{sub} \neq \beta_{sub} \end{cases} \tag{18}$$

$$T_c = \begin{cases} T_{c,i} + \alpha_{sub}(T_{c,i} - T_{w,i})x, & \alpha_{sub} = \beta_{sub} \\ T_{c,i} + \left(\dfrac{\beta_{sub}}{\alpha_{sub} - \beta_{sub}}\right)(T_{c,i} - T_{w,i})(1 - e^{(\beta_{sub} - \alpha_{sub})x}), & \alpha_{sub} \neq \beta_{sub} \end{cases} \tag{19}$$

Similarly, the solutions for the tube wall inner and outer surface temperatures are deduced from Eqs. 11-12, in conjunction with the above two expressions; i.e.,

$$T_{b,w} = T_w + \frac{\xi_{sub}}{h_w R_{T,i}}(T_c - T_w) \tag{20}$$

$$T_{b,c} = T_{b,w} + \frac{\xi_{sub}\ln(R_{T,o}/R_{T,i})}{k}(T_c - T_w) \tag{21}$$

Equations 18-21 are valid as long as the bulk water temperature remains below saturation. Past this point, boiling will ensue in the channel and the assumption of single phase forced convection heat transfer on the tube side is no longer valid. The length of this inlet subcooling region is evaluated from Eq. 18 by setting $T_w = T_{sat}$ and solving for x, which yields:

$$L_{sub} = \begin{cases} \dfrac{\Delta T_{sub}}{\alpha_{sub}(T_{c,i} - T_{w,i})}, & \alpha_{sub} = \beta_{sub} \\ \left(\dfrac{1}{\beta_{sub} - \alpha_{sub}}\right)\ln\left(\dfrac{\alpha_{sub}(T_{c,i} - T_{sat}) + \beta_{sub}\Delta T_{sub}}{\alpha_{sub}(T_{c,i} - T_{w,i})}\right), & \alpha_{sub} \neq \beta_{sub} \end{cases} \tag{22}$$

Equations 18-22 provide the complete set of solutions for the temperature evolution in the subcooled inlet region to the HX. The solutions for the saturated boiling region are developed in the next subsection.

Saturated Boiling Region

The coordinate system and nomenclature for this phase of the modeling are shown in Figures 2 and 3. In this region, boiling heat transfer will begin, leading to a significant augmentation in the overall heat transfer coefficient to the water coolant. A detailed analysis of this region would include the evaluation of the boiling characteristics from onset of nucleate boiling at the tube wall, on through bubbly and churn-turbulent flow regimes, and finally terminating in an annular flow regime in which the remaining liquid phase would undergo vaporization as a thin liquid film on the tube wall. A detailed analysis of this region is beyond the current scope of work. Rather, it is assumed that onset of boiling leads to a significant increase in the heat transfer coefficient from the tube inner surface to the two-phase flow mixture such that the heat transfer is limited predominately by conduction across the tube wall and, to a lesser extent, convection to the liquid metal. Although this assumption will lead to a slight under-prediction in the overall length of the saturated boiling zone, it significantly simplifies the modeling approach, and is also consistent with the scoping nature of this model.

Given the above assumptions, then the onset of boiling at the tube inner surface effectively fixes the surface temperature at the coolant saturation temperature, T_{sat}. Moreover, the two-phase coolant mixture temperature is effectively held constant at the saturation temperature. Under these conditions, the energy balance at the tube outer surface takes the form:

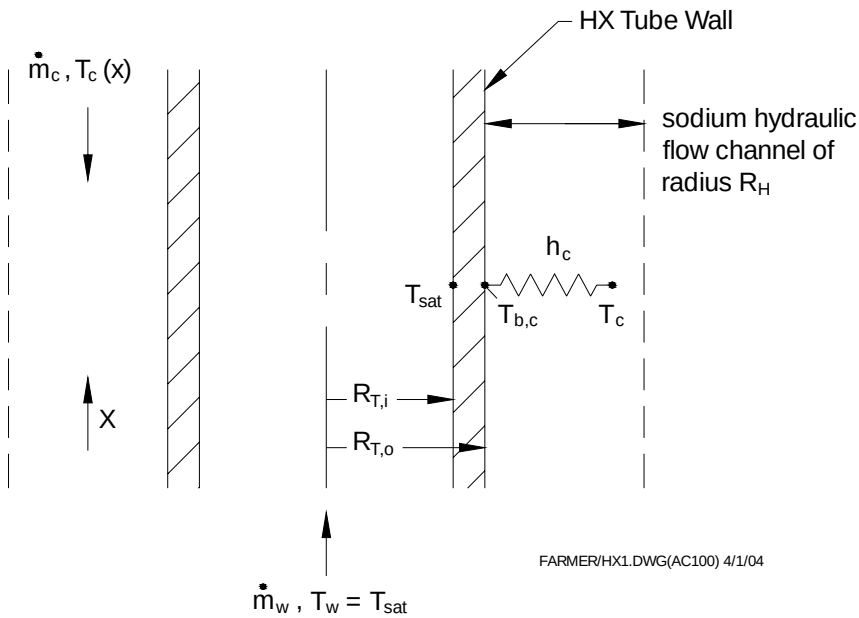

Figure 2. Depiction of geometry and nomenclature for saturated flow boiling region.

$$h_c(T_c - T_{b,c}) = \frac{k(T_{b,c} - T_{sat})}{R_{T,o}\ln(R_{T,o}/R_{T,i})} \tag{23}$$

Thus, the differential equation governing the evolution of the liquid metal temperature in the saturated boiling region is of the form:

$$\frac{dT_c}{dx} = \beta_{sat}(T_c - T_{sat}) \tag{24}$$

where:

$$\beta_{sat} = \frac{2\pi\xi_{sat}}{\dot{m}_c\, c_c} \tag{25}$$

$$\xi_{sat} = \frac{h_c k}{h_c \ln(R_{T,o}/R_{T,i}) + k/R_{T,o}} \tag{26}$$

The initial condition on Eq. 24 is deduced by requiring continuity of the liquid metal temperature with that at the end of the subcooled inlet region. In particular, the initial condition is deduced from Eqs. 19 and 22 as:

$$T_c\Big|_{x=L_{sub}} = T_{c,i} + \left(\frac{\beta_{sub}}{\alpha_{sub}}\right)\Delta T_{sub} \tag{27}$$

Thus, the solutions for the two-phase coolant and liquid metal temperatures in the saturated boiling region are found as:

$$T_w = T_{sat} \tag{28}$$

$$T_c = T_{sat} + \left[T_{c,i} + \left(\frac{\beta_{sub}}{\alpha_{sub}} \right) \Delta T_{sub} - T_{sat} \right] e^{\beta_{sat}(x - L_{sub})} \tag{29}$$

The solutions for the tube wall inner and outer surface temperatures are then deduced from Eqs. 23 and 28 as:

$$T_{b,w} = T_{sat} \tag{30}$$

$$T_{b,c} = \frac{h_c T_c \ln(R_{T,o} / R_{T,i}) + k T_{sat} / R_{T,o}}{h_c \ln(R_{T,o} / R_{T,i}) + k / R_{T,o}} \tag{31}$$

The length of the saturated boiling region is found by requiring that the net energy reduction in the liquid metal is sufficient to remove the latent heat of vaporization in the adjacent two-phase coolant mixture; i.e.,

$$\dot{m}_c \, c_c \left[T_c \Big|_{x = L_{sat} + L_{sub}} - T_c \Big|_{x = L_{sub}} \right] = \dot{m}_w \, h_{lv} \tag{32}$$

With Eqs. 27 and 32, the explicit requirement on the bulk liquid metal temperature at the end of the saturated boiling region is thus found as:

$$T_c \Big|_{x = L_{sat} + L_{sub}} = T_{c,i} + \left(\frac{\beta_{sub}}{\alpha_{sub}} \right) \Delta T_{sub} + \frac{\dot{m}_w h_{lv}}{\dot{m}_c \, c_c} \tag{33}$$

The length of the saturated boiling zone is then found by substituting the above equation into Eq. 29 and solving for x, which yields:

$$L_{sat} = L_{sub} + \frac{1}{\beta_{sat}} \ln \left\{ 1 + \frac{\dot{m}_w \, h_{lv}}{\dot{m}_c \, c_c \left[T_{c,i} + \left(\frac{\beta_{sub}}{\alpha_{sub}} \right) \Delta T_{sub} - T_{sat} \right]} \right\} \tag{34}$$

Equations 28-31 and 34 provide the complete set of solutions for the temperature evolution in the saturated boiling region of the HX. The solutions for the superheated steam flow region are developed in the next subsection.

Superheated Steam Flow Region

The coordinate system and nomenclature for this phase of the modeling are also shown in Figures 1 and 2. A straightforward analysis indicates that the differential equations governing the temperature evolution of the liquid metal and superheated steam in this region are identical in form to those developed for the subcooled inlet region. However, the thermophysical properties in the vapor region are evaluated using steam data (as opposed to water), and the inlet boundary conditions are redefined to be consistent with the exit conditions in the saturated boiling region. In particular, the differential equations governing the liquid metal and steam temperatures are of the form:

$$\frac{dT_w}{dx} = \alpha_{\sup}(T_c - T_w) \tag{35}$$

$$\frac{dT_c}{dx} = \beta_{\sup}(T_c - T_w) \tag{36}$$

where:

$$\alpha_{\sup} = \frac{2\pi\xi_{\sup}}{\dot{m}_w c_v} \tag{37}$$

$$\beta_{\sup} = \frac{2\pi\xi_{\sup}}{\dot{m}_c c_c} \tag{38}$$

$$\xi_{\sup} = \frac{h_c}{R_{T,i}} + \frac{h_v}{R_{T,o}} + \frac{h_c h_v}{k}\ln(R_{T,o}/R_{T,i}) \tag{39}$$

where:

h_v = convective heat transfer coefficient from steam to the tube wall.

The initial conditions on Eqs. 35 and 36 are given by Eqs. 28 and 33, respectively. Integration of this set of equations leads to the following solutions for the liquid metal and steam in the superheated steam flow region:

$$T_w = \begin{cases} T_{sat} + \alpha_{\sup}\left[T_{c,i} - T_{w,i} + \dfrac{\dot{m}_w h_{lv}}{\dot{m}_c c_c}\right](x - L_{sat} - L_{sub}), \alpha_{\sup} = \beta_{\sup} \\ T_{sat} + \left(\dfrac{\alpha_{\sup}}{\alpha_{\sup} - \beta_{\sup}}\right)\left(T_{c,i} - T_{sat} + \left(\dfrac{\beta_{sub}}{\alpha_{sub}}\right)\Delta T_{sub} + \dfrac{\dot{m}_w h_{lv}}{\dot{m}_c c_c}\right)\left(1 - e^{(\beta_{\sup} - \alpha_{\sup})(x - L_{sat} - L_{sub})}\right), \alpha_{\sup} \neq \beta_{\sup} \end{cases} \tag{40}$$

$$T_c = \begin{cases} T_{c,i} + \Delta T_{sub} + \dfrac{\dot{m}_w h_{lv}}{\dot{m}_c c_c} + \alpha_{\sup}\left[T_{c,i} - T_{w,i} + \dfrac{\dot{m}_w h_{lv}}{\dot{m}_c c_c}\right](x - L_{sat} - L_{sub}), & \alpha_{\sup} = \beta_{\sup} \\ T_{c,i} + \left(\dfrac{\beta_{sub}}{\alpha_{sub}}\right)\Delta T_{sub} + \dfrac{\dot{m}_w h_{lv}}{\dot{m}_c c_c} + \left(\dfrac{\beta_{\sup}}{\alpha_{\sup} - \beta_{\sup}}\right) \bullet & \\ \left(T_{c,i} - T_{sat} + \left(\dfrac{\beta_{sub}}{\alpha_{sub}}\right)\Delta T_{sub} + \dfrac{\dot{m}_w h_{lv}}{\dot{m}_c c_c}\right)\left(1 - e^{(\beta_{\sup} - \alpha_{\sup})(x - L_{sat} - L_{sub})}\right), & \alpha_{\sup} \neq \beta_{\sup} \end{cases} \tag{41}$$

Similarly, the solutions for the tube wall inner and outer surface temperatures in this region are found as:

$$T_{b,w} = T_w + \frac{\xi_{\sup}}{h_v R_{T,i}}(T_c - T_w) \tag{42}$$

$$T_{b,c} = T_{b,w} + \frac{\xi_{\sup} \ln(R_{T,o} / R_{T,i})}{k}(T_c - T_w) \tag{43}$$

As described earlier, the key objective of this work was to develop a model for predicting the required HX tube length to achieve a given steam superheat. This solution is found from Eq. 40 by setting the steam temperature to the specified superheat and solving for x, which yields:

$$L_{\sup} = L_{sub} + L_{sat} + \begin{cases} \dfrac{\Delta T_{\sup}}{\alpha_{\sup}\left(T_{c,i} - T_{w,i} + \dfrac{\dot{m}_w h_{lv}}{\dot{m}_c c_c}\right)}, \alpha_{\sup} = \beta_{\sup} \\ \left(\dfrac{1}{\beta_{\sup} - \alpha_{\sup}}\right)\ln\left(1 + \left(\dfrac{\beta_{\sup} - \alpha_{\sup}}{\alpha_{\sup}}\right)\dfrac{\Delta T_{\sup}}{\left[T_{c,i} - T_{sat} + \left(\dfrac{\beta_{sub}}{\alpha_{sub}}\right)\Delta T_{sub} + \dfrac{\dot{m}_w h_{lv}}{\dot{m}_c c_c}\right]}\right), \alpha_{sub} \neq \beta_{sub} \end{cases} \tag{44}$$

Equations 40-44 provide the complete set of solutions for the temperature evolution in the superheated steam flow region of the HX. With this step completed, the key aspects of the model have been fully documented. However, before actual calculations can be carried out, the convective heat transfer coefficients on the shell and tube sides of the HX need to be specified. Recommendations for these coefficients are provided in the next sub-section.

Correlations for Convective Heat Transfer Coefficients

The particular form of the heat transfer coefficients used in the previously described model depend upon the HX flow geometry. For instance, different expressions would be deployed for a helical coil tube arrangement versus the classic straight tube design. Or, for the straight tube design, detailed specification of the coefficients on the shell side would depend upon whether the tubes were configured in a square versus triangular pitch. However, for the purposes of this scoping model, the correlations that are recommended are for a simple pipe flow geometry in which the characteristic scale is set equal to the channel hydraulic diameter (i.e., four times the flow area divided by the wetted perimeter of the channel).

On the tube side of the HX in the subcooled inlet region, the convective heat transfer coefficient is evaluated using the classic Dittus-Boelter correlation, which is of the form:

$$h_w = \begin{cases} \dfrac{7.6k_w}{D_{T,i}}, & \mathrm{Re}_w \le 2300 \\ \\ 0.023\mathrm{Re}_w^{0.8}\,\mathrm{Pr}_w^{0.4}\left(\dfrac{k_w}{D_{T,i}}\right), & \mathrm{Re}_w > 2300 \end{cases} \tag{45}$$

where:

$D_{T,i}$ = HX tube ID = $2R_{T,i}$,

Pr_w = Prandtl number of water coolant = $\dfrac{\mu_w c_w}{k_w}$,

Re_w = Reynolds number of coolant = $\dfrac{\rho_w u_w D_{T,i}}{\mu_w} = \dfrac{4\dot{m}_w}{\pi\mu_w D_{T,i}}$,

u_w = coolant flow velocity,

ρ_w = coolant density,

k_w = coolant thermal conductivity, and

μ_w = coolant viscosity.

In the superheated steam flow region, the convective heat transfer coefficient on the tube side is also evaluated with the Dittus-Boelter correlation, except that the thermo-physical properties are evaluated using steam data; i.e.,

$$h_v = \begin{cases} \dfrac{7.6k_v}{D_{T,i}}, & \mathrm{Re}_v \le 2300 \\ \\ 0.023\mathrm{Re}_v^{0.8}\,\mathrm{Pr}_v^{0.4}\left(\dfrac{k_v}{D_{T,i}}\right), & \mathrm{Re}_v > 2300 \end{cases} \tag{46}$$

where:

Pr_v	=	Prandtl number of steam $= \dfrac{\mu_v c_v}{k_v}$,
Re_v	=	Reynolds number of steam $= \dfrac{\rho_v u_v D_{T,i}}{\mu_v} = \dfrac{4\dot{m}_w}{\pi \mu_v D_{T,i}}$,
u_v	=	steam flow velocity,
ρ_v	=	steam density,
k_v	=	steam thermal conductivity, and
μ_v	=	steam viscosity.

On the shell side of the HX, the convective heat transfer coefficient is evaluated using the classic Martinelli correlation that was developed for liquid metal flow in tubes. The correlation is of the form:

$$h_c = \left[5.0 + 0.025\left(\mathrm{Re}_c\,\mathrm{Pr}_c\right)^{0.8}\right]\left(\frac{k_c}{D_H}\right) \tag{47}$$

where:

D_H	=	HX shell side sub-channel hydraulic diameter,
Pr_c	=	Prandtl number of liquid metal $= \dfrac{\mu_c c_c}{k_c}$,
Re_c	=	Reynolds number of liquid metal $= \dfrac{\rho_c u_c D_H}{\mu_c} = \dfrac{4\dot{m}_c}{\pi \mu_c D_H}$,
u_v	=	liquid metal flow velocity,
ρ_v	=	liquid metal density,
k_v	=	liquid metal thermal conductivity, and
μ_v	=	liquid metal kinematic viscosity.

Note that Eq. 47 is valid for both laminar and turbulent flows.

The HX sub-channel hydraulic diameter in Eq. 47 is a design-specific parameter that is left as a user-specified input variable. For instance, if the HX is based on a square-pitch tube

design, then the hydraulic diameter is evaluated in terms of the pitch and the tube OD through the expression:

$$D_H = \frac{4 \bullet \textit{flow area}}{\textit{wetted perimeter}} = \frac{P^2 - \pi D_{T,o}^2 / 4}{\pi D_{T,o}} \tag{48}$$

where:

P	=	tube pitch, and
$D_{T,o}$	=	HX tube OD = $2R_{T,o}$

With the shell and tube side convective heat transfer coefficients defined through Eqs. 45-48, the model for evaluating the required HX tube length to achieve a given steam superheat is fully specified. To illustrate the model application, a representative calculation for the AFR-300 design is provided in the next section.

Sample Application to the AFR-300 Design

To illustrate the application of the model, a sample calculation is provided for the intermediate heat transport system of the AFR-300. The input data for the model are fully specified in Table 1. The HX thermal power rating and sodium inlet and exit temperatures are selected to be consistent with the reference IHX characteristics (see Table 5 in the reference). The tube side operating pressure of 7 MPa (~1000 psia), tube diameter, and pitch are arbitrarily specified, but the selected values are consistent with other current HX designs.

Key model results are summarized in Table 2, while the spatial evolution of temperatures across the HX is shown are Figures 4 and 5. As shown in Table 2, the required HX tube length to achieve a 50 ºC steam superheat is calculated to be 3.23 m, with most of this length (i.e., 1.93 m) devoted to removal of the water latent heat in the saturated flow boiling region. As shown in Table 1, the assumed sub-channel hydraulic diameter is 2.0 cm, which yields a tube pitch of 3.1 cm from Eq. 48 for a square pitch array. Thus, given that there are 3000 tubes assumed in the HX design (see Table 1), then the overall dimensions of this 267 MWt HX would by ~ 1.9 m in diameter and 3.2 m high.

Examination of the temperature profile data in Figures 4 and 5 indicates that the peak temperature differential across the tube wall occurs at the end of the saturated boiling region (i.e., at 2.61 m from the bottom of the HX). Here, the temperature differential approaches 120 ºC. The discontinuous jump in the tube inner surface temperature at this location is due to the fact that the heat transfer mechanism changes abruptly from forced convection boiling to a single phase forced convection heat transfer regime. Thus, the tube inner surface temperature must re-adjust at this location to account for the relatively low heat transfer coefficient to the flowing steam.

Table 1. Summary of model input data.

Input Parameter	Model Symbol	Value
Core/HX Thermal Rating	P_{core}	267 MWt
Tube side saturation temperature (corresponding operating pressure)	T_{sat}	286 ºC (7 MPa)
Feedwater inlet subcooling	ΔT_{sub}	20 ºC
Steam exit superheat	ΔT_{sup}	50 ºC
Core liquid metal inlet temperature (equivalent to HX exit temperature)	$T_{c,i}$	315 ºC
Core liquid metal exit temperature (equivalent to HX inlet temperature)	$T_{c,o}$	488 ºC
Number of HX tubes	N_T	3000
Tube OD	$D_{T,o}$	1.32 cm
Tube wall thickness	t_w	2.00 mm
Tube thermal conductivity	k	35 W/m-ºC
Sub-channel hydraulic diameter	D_H	2.00 cm
Sodium density	k_c	832 kg/m^3
Sodium viscosity	μ_c	$2.76 \cdot 10^{-4}$ kg/m-s
Sodium thermal conductivity	k_c	69.4 W/m-ºC
Sodium specific heat	c_c	1283 J/kg- ºC
Water specific enthalpy at saturation conditions (7 MPa)	e_{liq}	1.267 MJ/kg
Water latent heat of vaporization (7 MPa)	h_{lv}	1.505 MJ/kg
Water density	ρ_w	740 kg/m^3
Water viscosity	μ_w	$9.2 \cdot 10^{-5}$ kg/m-s
Water thermal conductivity	k_w	0.65 W/m-ºC
Water specific heat	c_w	5600 J/kg- ºC
Steam density	ρ_v	36.5 kg/m^3
Steam viscosity	μ_v	$1.9 \cdot 10^{-5}$ kg/m-s
Steam thermal conductivity	k_v	0.06 W/m-ºC
Steam specific heat	c_v	4300 J/kg- ºC

Table 2. Key model results.

Output Variable	Model Symbol	Value
Total core/HX sodium flowrate	$\dot{m}_{core}$	1202.9 kg/s
Total HX feedwater flowrate	$\dot{m}_{w,HX}$	145.7 kg/s
Sub-channel shell-side sodium flowrate	$\dot{m}_c$	0.40 kg/s
Sub-channel tube-side water flowrate	$\dot{m}_w$	0.049 kg/s
Sub-channel shell-side liquid metal heat transfer coefficient	h_c	29.3 kW/ m^2-ºC
Sub-channel heat transfer coefficient in inlet subcooling region	h_w	11.5 kW/ m^2-ºC
Sub-channel heat transfer coefficient in steam superheat region	h_v	4.6 kW/ m^2-ºC
Characteristic thermal resistance of tube wall	k/t_w	17.5 kW/ m^2-ºC
Differential length of inlet subcooling region	L_{sub}	0.68 m
Differential length of saturated flow boiling region	$L_{sat} - L_{sub}$	1.93 m
Differential length of superheated steam flow region	$L_{sup} - L_{sat} - L_{sub}$	0.62 m
Total HX tube length to achieve 50 ºC steam superheat	L_{sup}	3.23 m

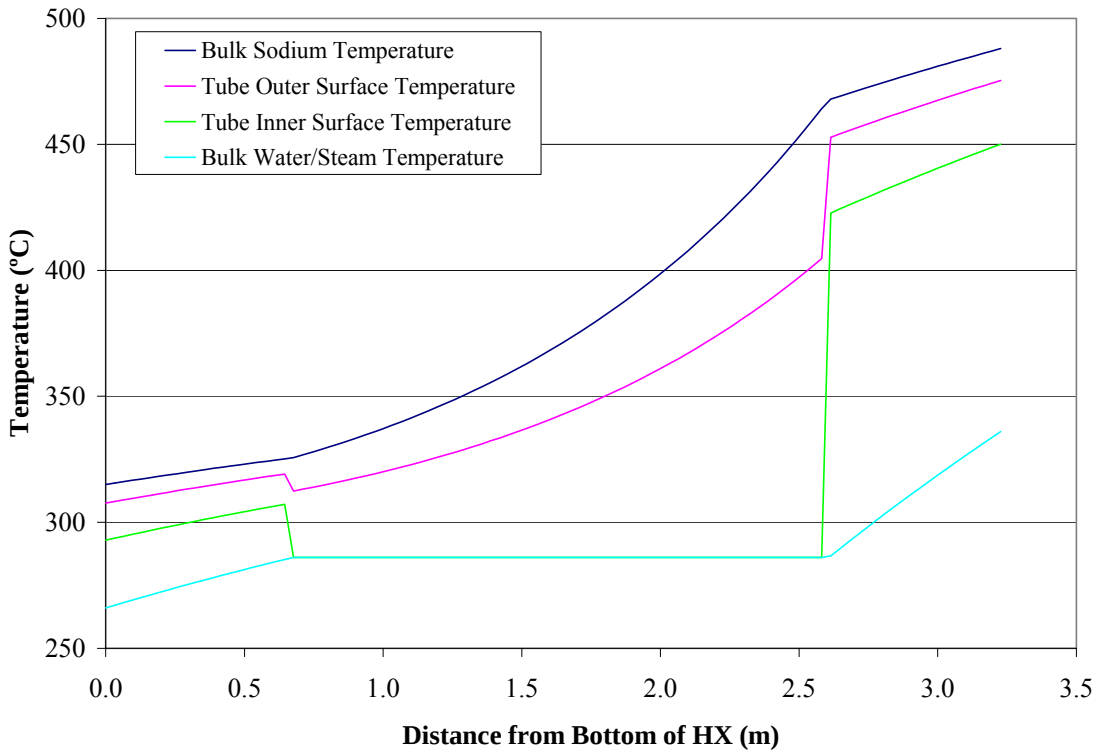

Figure 4. Calculated temperatures vs. distance from bottom of the HX.

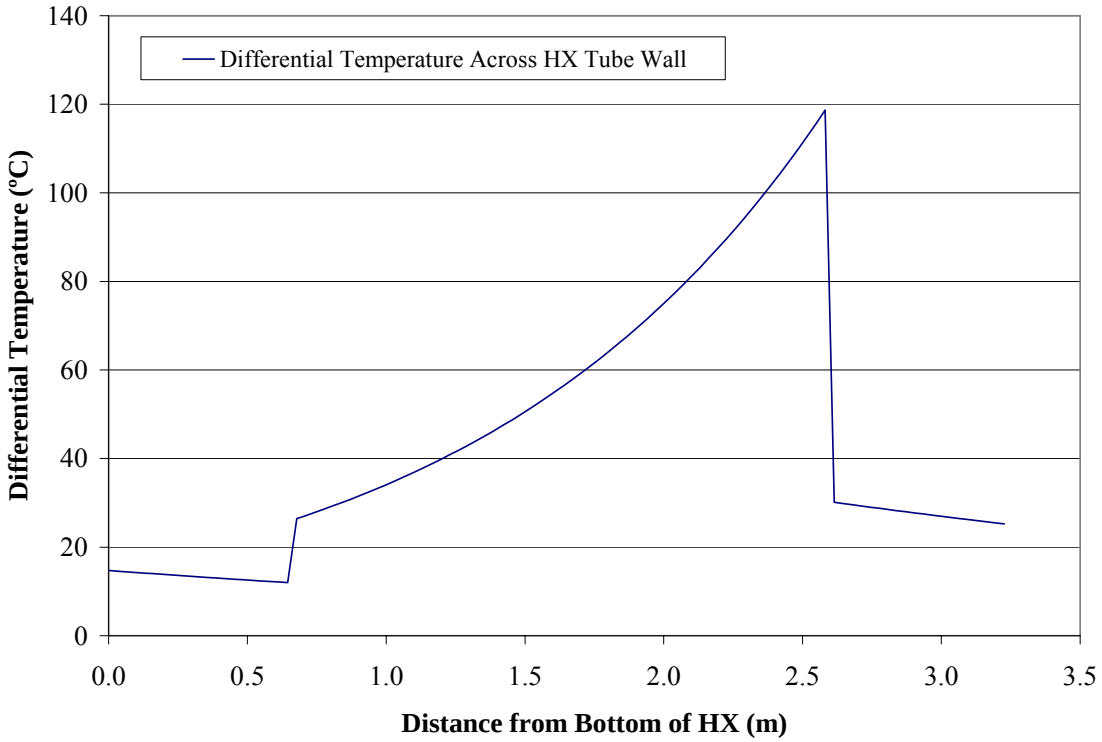

Figure 5. Temperature difference across tube wall vs. distance from the bottom of the HX.

Further examination of Figure 4 reveals a few limitations in the model. In particular, due to the comparatively low value of the forced convection heat transfer coefficient on the tube side in the inlet subcooling region, the calculated tube inner wall surface temperature is above the assumed saturation temperature of 286 ºC. Thus, subcooled flow boiling would occur in this inlet region, as opposed to the assumed single-phase forced convection heat transfer regime. The onset of boiling in the inlet region would effectively limit the inner surface temperature to within a few degrees of the saturation temperature. Furthermore, onset of boiling would increase the tube-side heat transfer coefficient, which would shorten the length of this inlet region.

MF:mg

cc: C. Grandy
J. Sienicki
NE Files:
EDL Files:

APPENDIX B

EVALUATION OF SIMPLIFIED THERMAL-HYDRAULIC MODEL
FOR SHELL-AND-TUBE STEAM GENERATOR

ARGONNE NATIONAL LABORATORY
9700 South Cass Avenue, Argonne, Illinois 60439-4841 INTRA-LABORATORY MEMO

April 26, 2004

TO: S. A. Kamal N.E.

FROM: A. R. Brunsvold N.E.

Subject: **Evaluation Efforts on a Simplified Thermal-Hydraulics Model for a Shell-and-Tube Steam Generator and Recommended Input Parameters for the Base Case and High Temperature Designs**

References:

1. Draft Intra-Laboratory Memo, "Thermal-Hydraulics Model for Shell-and-Tube Type Superheated Steam Generator," Mitch Farmer to Sami Kamal, Dated April 5, 2004.

2. J. S. McDonald, A. Andonedis, J Matte III, Atomics International / Burns and Roe / ERDA-EPRI, Unpublished information, May 1977.

3. K. Kim and J. R. Faitel, Rockwell International, Unpublished information, June 1984.

4. C. W. Grandy et al., Argonne National Laboratory, Unpublished information, October 2002.

Introduction

This memo summarizes the efforts to evaluate the steam generator model described in Ref. 1. The Ref. 1 model will be referred to in this memo as the SG Model. It is concluded on the basis of the evaluation summarized below that the SG Model represents the behavior of a once through steam generator with reasonable accuracy within the simplifying assumptions used. The model and assumptions are discussed below.

Recommended input for operating parameters are made for a base case consistent with the AFR-300 (Ref. 4) plant design. Recommendations are also made for future improvements to the SG Model.

Discussion

As described in Ref. 1 the thermal-hydraulics of a counter-flow shell-and-tube sodium heated steam generator is modeled as a single tube-in-tube counter-flow heat exchanger with water/steam on the tube side.

The tube side thermal hydraulics are represented in three regions, a sub-cooled region, a boiling region, and a superheated region. The SG Model does not account for pressure drops. The sodium and water/steam are assumed to remain at their respective inlet pressures throughout.

The water side heat transfer in the sub-cooled region is assumed to be single phase meaning no boiling occurs at the tube ID while the bulk water temperature is below saturation. The water/steam heat transfer in the boiling region is modeled by assuming the ID surface of the tube is at the saturation temperature of the water/steam until the fluid becomes superheated.. The SG Model does not include a film boiling region.

The physical properties of the fluids and tube are given as input to the SG Model program. The sodium properties and the tube properties are assumed constant. The water/steam properties are assumed constant in each of the three regions included in the SG Model. The heat transfer coefficients used in the SG Model are obtained from common, well known correlations, are consistent with the modeling assumptions and are suitable to the purpose.

The simplifying assumptions described above will, as Ref. 1 notes, result in underestimating the heat transfer area required for a given set of a steam generator operating conditions. For the purpose the SG Model will be used this is not considered of overriding importance. The SG Model will be used in trade studies to determine the advantages, if any, of using alternate materials and/or operating conditions with a given steam generator design. For this purpose predicting correct trends is more important than predicting the final size of the steam generator. The SG Model is expected to predict trends reasonably well for comparison purposes.

Evaluation

The efforts to evaluate the SG Model have been made on the basis of two considerations, 1) a comparison of the SG Model predicted general results to the results reported for a steam generator design with extensive development and testing basis (referred to below as the Bench Mark), and 2) evaluating the predicted behavior of the fluid and tube wall temperature distributions along the length of the steam generator for correct trends.

The bench mark SG results are taken from Ref. 2. The steam generator design of Ref. 2 was a sodium-heated, once-through, counter-flow, hockey-stick, single-wall tube configuration with water on the tube side. The unit described in Ref. 2 was designed specifically for once through operating conditions. The bench mark design was completed by Atomics International (AI) using the same diameter tubes as used in the Clinch River Breeder Reactor (CRBR) steam generator modules. The active heat transfer region of the hockey stick tube bundle is confined to the long leg of the steam generator. Thus, for heat transfer purposes, the hockey stick is correctly modeled as a straight tube unit.

Note that one of the CRBR modules was tested in the ETEC SG Test Facility from 20 to the 40% of full power rating per tube for once through operating conditions (Ref. 3).

Input for the Bench Mark parameters for the SG Model are given in Table 1. A comparison of the results using the SG Model with those of AI found in Ref. 2 are given in Table 2. The table is organized with parameters used as input to the SG Model given in the upper rows by those calculated by the SG Model. A comparison of the Table 2 flow rates and the active heat transfer length shows the following:

Sodium Flow Rate: The sodium flows are very close with the SG Model predicting a flow that is greater than the AI value by less than 1%.

Water/Steam Flow Rate: The SG Model predicts the water/steam flow rate to be about 8% greater than the AI water/steam flow rate. This difference is attributed primarily to the differences in the water/steam properties used in the two studies which result from the simplifications made in the SG Model. The major simplifications in the SG Model are the assumption of constant water/steam side pressure and the use of constant specific heats at representative temperatures in the subcooled and superheated regions.

Active Heat Transfer Length: The SG Model predicts an active heat transfer length that is about 26% less than the length given by AI. This under-prediction is expected. The reasons the SG Model predictions are low are partly due to the modeling simplifications and also due to the fact that the SG Model does not include any allowances for uncertainties and/or reliability that were included in the AI steam generator design. These are summarized below along with the authors estimate of the magnitude.

- The SG Model assumes pure counter flow on the shell side of the unit. The AI design is not pure counter flow and the design very likely includes some allowance to account for this.
  (Est. 1 - 3 %)
- The SG Model does not account for sub-cooled boiling in the sub-cooled region and does not include film boiling the in the boiling region. These simplifications have the opposite effect but neglecting the film boiling region is expected to be the more serious. This will result in a under predicting the active heat transfer length.
  (Est. 2 - 5 %)
- The SG Model does not account for an ineffective heat transfer region where the tubes pass through support plates.
  (Est. 1 - 2 %)
- The SG Model does not include a tube plugging allowance. The AI design included a plugging allowance.
  (Est. 2 - 3 %)
- The SG Model does not include a water-side fouling allowance.

(Est. 2 - 4 %)

- The SG Model does not include allowance for the accumulation of uncertainties such as, manufacturing allowances, thermal physical properties, heat transfer coefficients, etc.

  (Est. 10 - 20 %)

The estimate of uncertainties as outlined above total to a range from 18 to 37 %. Thus it is concluded that the SG Model calculated active heat transfer length which is 26% below the length given by AI is within the expected the modeling assumptions plus the margin included in the AI design.

Fig. 1 shows the tube and both fluid temperature profiles along the active heat transfer length for the AI Hockey Stick SG calculated by the SG Model for the input given in Table 1. The results appear reasonable considering the simplifying assumptions.

The simplification that is most notable is the neglect of a water/steam film boiling region on the tube wall temperature differences. Because the tube ID surface is assumed to remain at the saturation temperature throughout the boiling region the large change in the tube wall temperature difference occurs at the transition from the boiling region to the superheat region. The tube wall temperature difference profile is shown Fig. 1 (the lowest temperature profile). As shown in Fig. 1, at about 11.5 m, the tube wall delta T is about 51 C at the end of the boiling region and drops to about 19 C at the beginning of the superheat region. The 51 C delta T would not be as large if a film boiling region were included in the SG Model. Using the delta T's occurring at this transition as a first estimate of the effect of departure from nucleate boiling at some point before 100% quality is reached in the boiling region is expected to be conservative. That is, the actual delta-delta T difference would be expected to be smaller than shown in Fig. 1.

Input Parameters for Trade Studies

Recommended input parameters for the SG Model to perform preliminary predictions for two examples of possible steam generator operating conditions are included in this memo as discussed below.

<u>AFR-300 Base Case</u>

The steam generator design used for the AFR-300 plant study (Ref. 4) was a shell-and-tube, counter flow, steam generator with the water/steam on the tube side. The tubes were straight double-walled tubes fabricated from 2-1/4Cr-1Mo.

Table 3 gives the recommended input parameters for the SG Model for a single-walled straight tube steam generator configuration for the AFR-300 operating conditions.

<u>Higher Temperature Steam Generator</u>

For the purpose of evaluating the use of a higher temperature and materials that would accompany higher temperature a set of input parameters are given for the case of raising the steam outlet temperature from that used by AFR-300, 457 C (855 F), to 538 C (1000F). This set of input parameters is given in Table 4.

Conclusion

The SG Model predicts reasonable results which can be used to make trade studies on once through steam generators by careful consideration of the simplifying assumptions used in the model.

Recommendations

Recommended future improvements to the SG Model are given below.

1. Include a film boiling region,
2. Include temperature and pressure dependant thermal/physical properties,
3. Include a subcooled boiling region.

Table 1. Bench Mark Input for the SG Model

Operating Parameters		
Thermal Rating	MW	292
Tube Side Saturation T (P)	C (MPa)	347 (16)
Feedwater Inlet Subcooling	C	104
Steam Exit Superheat	C	110
SG Na Exit T	C	315
SG Na Inlet T	C	482
SG Geometric & Tube Data		
Number of Tubes		2200
Tube ID	cm	1.034
Tube Wall Thickness	mm	2.77
Tube OD	cm	1.59
Sub-channel Hydraulic Diameter	cm	4.15
Tube Material		2.25Cr-1Mo
Tube Thermal Conductivity	W/m-C	36
Fluid Properties		
Na Density	kg/m^3	856
Na Viscosity	kg/m-s	2.8E-04
Na Thermal Conductivity	W/m-C	71.6
Na Specific Heat	J/kg-C	1280
Water Specific Enthalpy at Sat Condition	MJ/kg	1.65
Water Latent Heat of Vaporization	MJ/kg	0.931
Water Density	kg/m^3	738
Water Viscosity	kg/m-s	9.06E-05
Water Thermal Conductivity	W/m-C	0.573
Water Specific Heat	J/kg-C	5330
Steam Density	kg/m^3	70
Steam Viscosity	kg/m-s	2.51E-05
Steam Thermal Conductivity	W/m-C	0.0843
Steam Specific Heat	J/kg-C	4491

Notes:

(1) The input parameters for the SG Model given above are consistent with the parameters given in Ref. 2 for the AI OTSG.

(2) The water and steam properties were taken from the NIST on-line data base (http://webbook.nist.gov/chemistry/fluid).

(3) The sodium properties were taken from "Thermal Physical Properties of Sodium," G. H. Golden, and J. V. Tokar, ANL-7323, 1967.

(4) The properties for the 2.25Cr-1Mo tubes were taken from NSMH Vol 1, Book 3, Property Code 3112.

Table 2. Comparison of Bench Mark Parameters and SG Model Predictions

SG Configuration		Counter Flow, Single Wall Water on Tube Side	
		Input Parameters	
		AI Hockey Stick OTSG (Ref. 2)	SG Model
Thermal Rating		292 MWt	
Na Temperature In		482 C (900 F)	
Na Temperature Out		315 C (600 F)	
Water Temperature In		243 C (470 F)	
Water Inlet Pressure		16.2 MPa (2350 psi)	16 MPa (2321 psi)[1]
Steam Temperature Out		457 C (855 F)	
Steam Outlet Pressure		15.7 MPa (2275 psi)	16 MPa (2321 psi)[1]
Tube OD		1.59 cm (0.625 in)	
Tube Wall Thickness		2.77 mm (0.109 in)	
Tube Pitch		2.87 cm (1.13 in)	
Number of Tubes		2200	
		Results	
Na Flow		1.36E+03 kg/s (10.8E+06 lb/hr)	1.37E+03 kg/s (10.9E+06 lb/hr)
Water/Steam Flow Rate		1.37E+02 kg/s (1.09E+06 lb/hr)	1.48E+02 kg/s (1.18E+06 lb/hr)
Active Heat Transfer Length		23.5 m (77 ft)	17.2 m (56.8 ft)

Note:

(1) The SG Model assumes the fluids remain at their respective inlet pressures throughout the unit.

Table 3. Input for the SG Model Base Case

Operating Parameters		
Thermal Rating	MW	267
Tube Side Saturation T (P)	C (MPa)	347 (16)
Feedwater Inlet Subcooling	C	120
Steam Exit Superheat	C	110
SG Na Exit T	C	315
SG Na Inlet T	C	488
SG Geometric & Tube Data		
Number of Tubes		2000
Tube ID	cm	1.11
Tube Wall Thickness	mm	2.83
Tube OD	cm	1.68
Sub-channel Hydraulic Diameter	cm	3.67
Tube Material		2.25Cr-1Mo
Tube Thermal Conductivity	W/m-C	36
Fluid Properties		
Na Density	kg/m^3	856
Na Viscosity	kg/m-s	2.8E-04
Na Thermal Conductivity	W/m-C	71.6
Na Specific Heat	J/kg-C	1280
Water Specific Enthalpy at Sat Condition	MJ/kg	1.65
Water Latent Heat of Vaporization	MJ/kg	0.931
Water Density	kg/m^3	747
Water Viscosity	kg/m-s	9.26E-05
Water Thermal Conductivity	W/m-C	0.581
Water Specific Heat	J/kg-C	5230
Steam Density	kg/m^3	70
Steam Viscosity	kg/m-s	2.51E-05
Steam Thermal Conductivity	W/m-C	0.0843
Steam Specific Heat	J/kg-C	4491

Note:

The input parameters for the SG Model given above are consistent with the parameters given in Ref. 4 for the AFR-300.

Table 4. Input for the SG Model High Temperature Case

Operating Parameters		
Thermal Rating	MW	267
Tube Side Saturation T (P)	C (MPa)	347 (16)
Feedwater Inlet Subcooling	C	37
Steam Exit Superheat	C	191
SG Na Exit T	C	399
SG Na Inlet T	C	566
SG Geometric & Tube Data		
Number of Tubes		2000
Tube ID	cm	1.11
Tube Wall Thickness	mm	5.73
Tube OD	cm	2.26
Sub-channel Hydraulic Diameter	cm	4.94
Tube Material		2.25Cr-1Mo
Tube Thermal Conductivity	W/m-C	34.9
Fluid Properties		
Na Density	kg/m^3	836
Na Viscosity	kg/m-s	2.43E-04
Na Thermal Conductivity	W/m-C	67.6
Na Specific Heat	J/kg-C	1265
Water Specific Enthalpy at Sat Condition	MJ/kg	1.65
Water Latent Heat of Vaporization	MJ/kg	0.931
Water Density	kg/m^3	657
Water Viscosity	kg/m-s	7.69E-05
Water Thermal Conductivity	W/m-C	0.502
Water Specific Heat	J/kg-C	6615
Steam Density	kg/m^3	59.9
Steam Viscosity	kg/m-s	2.69E-05
Steam Thermal Conductivity	W/m-C	0.0812
Steam Specific Heat	J/kg-C	3487

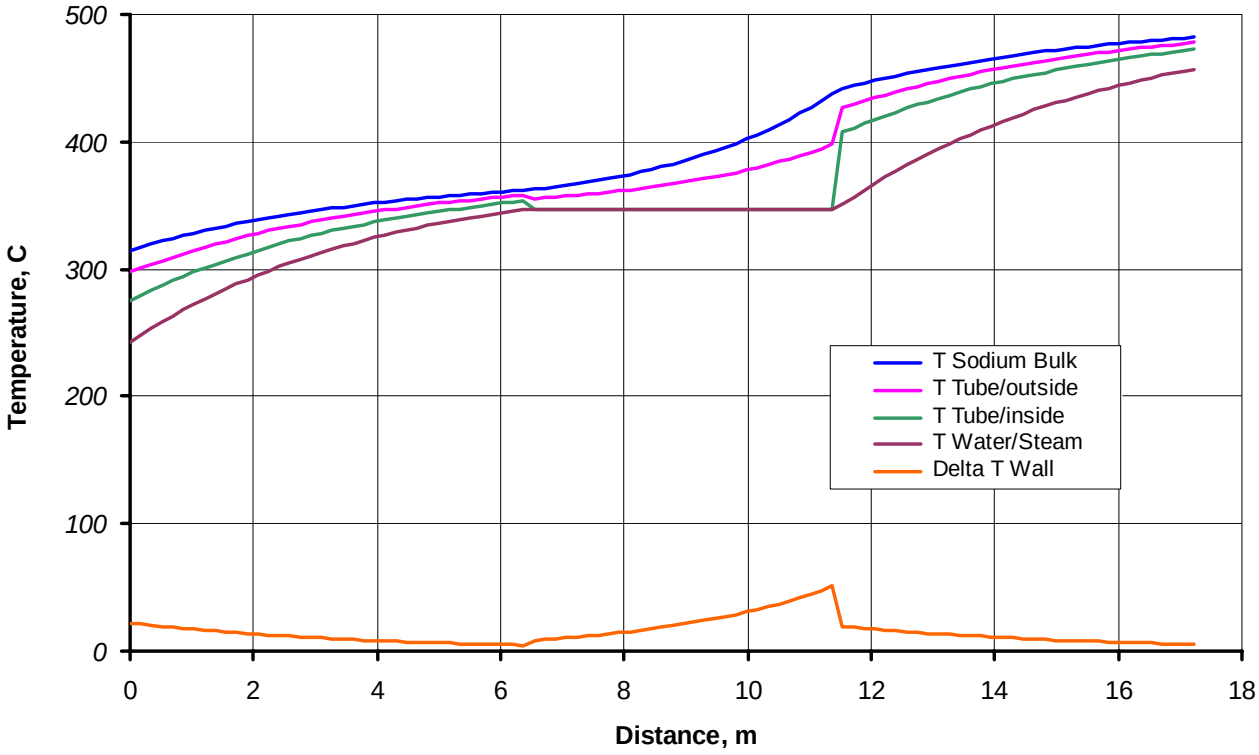

Figure 1. Temperature Profiles from the SG Model using Input Parameters from AI OTSG Design Study.

Attachment

cc:
C. Grandy
M. Farmer
File No. LDRD 2004-182